

# Hydraulic catheter device for treating chronic total occlusion

A feasibility study

J. Karapanagiotis

Technische Universiteit Delft



# Hydraulic catheter device for treating chronic total occlusion

A feasibility study

by

**J. Karapanagiotis**

in partial fulfillment of the requirements for the degree of

**Master of Science**

in Mechanical Engineering

Track: Precision and Microsystems Engineering

Specialisation in Mechatronic System Design

at the Delft University of Technology,  
to be defended publicly on Thursday November 16, 2017 at 2:30 PM.

Supervisor:	Ir. J. W. Spronck	
Thesis committee:	Ir. J. W. Spronck,	TU Delft
	Ir. A. Sakes,	TU Delft
	Dr. J. J. van den Dobbelsteen,	TU Delft
	Ir. S. G. E. Lampaert,	TU Delft

*This thesis is confidential and cannot be made public until November 30, 2022.*

An electronic version of this thesis is available at <http://repository.tudelft.nl/>.



# Abstract

Chronic total occlusion (CTO) occurs in approximately a third of all patients with coronary artery disease and is one of the most challenging types of conditions to treat. Minimally invasive methods like percutaneous coronary intervention (PCI) show a high treating potential as well as low costs, short hospital stay and fast recovery. However, their success rate is limited due to their mechanical force transmission, often leading to inability of crossing the hard proximal cap of the CTO. This study focuses on a promising non-mechanical concept for treating CTO using PCI. The proposed idea is based on energy transmission via hydraulic pressure waves in a liquid filled catheter tube. The aim of this project is to conduct a feasibility study for treating CTO by simulating a realistic situation based on the proposed concept. The first stage involved understanding the existing setup and dealing with its flaws and limitations. After the setup was improved and made appropriate for systematic experiments, a realistic scenario was simulated in the lab which led to a drop in force efficiency to one tenth of its original value, a useful result for estimating the required input force to puncture a real CTO. A CTO model was manufactured using gelatin and hydroxyapatite powder. In the final tests, the device was used to puncture effectively the CTO and demonstrate the feasibility of the concept in an *ex vivo* situation. Only one strike was enough to puncture the soft proximal caps whereas 2 to 4 strikes were needed for the hard caps. The input peak force was set to 36 N. Finally, the sensing capabilities of the device were explored with the purpose of getting information on the compliance of the target in contact with the output tip of the catheter.

*Keywords:* Coronary artery disease, chronic total occlusion, percutaneous coronary intervention, interventional cardiology, hydraulic pressure wave, biomedical device, catheter, load cell response.



# Preface

With this final part of my work as a student I would like to conclude my master education, which has been a fun and difficult journey of conscious effort. Although understanding is attained by self intent, it would have been impossible to complete this cycle without the help and support of certain people, to whom I personally want to pay tribute.

Firstly I would like to express my warmest appreciation to my supervisor Jo Spronck for criticising my work from the beginning and teaching me to doubt everything. I would also like to thank him for a great project idea; a biomedical device with the prospect of improving people's life kept me motivated and dedicated to my goal. In addition, I want to thank Aimée Sakes for her useful guidance and for giving me the opportunity to contribute in one of her academic publications. I would also like to thank John van den Dobbelsteen and Stefan Lampaert for being part of my thesis committee.

I wish to extend my thanks to the lab technicians and workshop employees, especially Rob Luttjeboer and Spiridon van Veldhoven for their invaluable help and patience in the Mechatronics Lab. Furthermore, the interesting discussions and insightful comments from the MSD group during our Monday meetings have been greatly appreciated.

Last but not least, I wish to express my profound gratitude to my family and friends for their support and encouragement in times of need.

*J. Karapanagiotis  
Rotterdam, October 2017*

*"Knowledge can be transmitted from one person to another, but it is impossible for someone to give understanding to someone else."*

—G. I. Gurdjieff



# Contents

<b>1</b>	<b>Introduction</b>	<b>1</b>
1.1	Background . . . . .	1
1.2	Aim & Objectives . . . . .	3
1.3	Thesis outline . . . . .	4
<b>2</b>	<b>Literature Review</b>	<b>5</b>
2.1	PCI State-of-the-Art . . . . .	5
2.2	Hydraulic pressure waves . . . . .	6
2.3	Contact mechanics . . . . .	7
2.4	Load cell model . . . . .	8
2.5	CTO properties . . . . .	10
<b>3</b>	<b>Existing Setup</b>	<b>11</b>
3.1	Hydraulic catheter . . . . .	12
3.2	Impulse . . . . .	13
3.2.1	Ideal vs real impulse . . . . .	13
3.2.2	Contacting surfaces . . . . .	13
3.2.3	Impulse measurement by load cell . . . . .	14
3.2.4	Impulse mechanism . . . . .	15
3.3	Load cells . . . . .	15
3.3.1	Sensor type and configuration . . . . .	15
3.3.2	Ringling effect . . . . .	16
<b>4</b>	<b>Improvement of Setup</b>	<b>19</b>
4.1	Avoiding air entrapment . . . . .	19
4.2	Load cell attachment . . . . .	20
4.3	Need for a membrane . . . . .	20
4.4	Orientation of output . . . . .	21
4.5	Adjustable input stroke . . . . .	21
<b>5</b>	<b>PCI Simulation</b>	<b>23</b>
5.1	Reference setup . . . . .	23
5.2	Step 1: Sliding of the output tip along the artery wall . . . . .	25
5.2.1	Simulation . . . . .	25
5.2.2	Results . . . . .	25
5.2.3	Conclusions . . . . .	25
5.3	Step 2: Material properties of the CTO proximal cap . . . . .	25
5.3.1	Simulation . . . . .	25
5.3.2	Results . . . . .	26
5.3.3	Conclusions . . . . .	26
5.4	Step 3: Connection of the CTO to the heart tissue . . . . .	27
5.4.1	Simulation . . . . .	27
5.4.2	Results . . . . .	27
5.4.3	Conclusions . . . . .	27
5.4.4	Step 3 with pre-load . . . . .	27
5.5	Step 4: Mass of the CTO . . . . .	28
5.5.1	Simulation . . . . .	28
5.5.2	Results . . . . .	28
5.5.3	Conclusions . . . . .	29
5.6	Artificial CTO replication . . . . .	29

---

<b>6</b>	<b>Target Compliance Sensing</b>	<b>35</b>
6.1	Overview . . . . .	35
6.2	Measurement Principle . . . . .	35
6.3	Experiment . . . . .	36
6.4	Results . . . . .	37
6.5	Conclusion and Discussion . . . . .	39
<b>7</b>	<b>Conclusions and Recommendations</b>	<b>41</b>
7.1	Conclusions . . . . .	41
7.2	Recommendations . . . . .	42
7.2.1	Effect of pre-load . . . . .	42
7.2.2	Effect of trapped air . . . . .	42
7.2.3	Pressure measurement . . . . .	42
7.2.4	Different actuation method . . . . .	43
7.2.5	Output modification . . . . .	43
7.2.6	Tissue compliance . . . . .	43
<b>A</b>	<b>Appendix A: Actuation mechanism</b>	<b>45</b>
<b>B</b>	<b>Appendix B: Results with membrane</b>	<b>47</b>
<b>C</b>	<b>Appendix C: CTO and device modelling results</b>	<b>49</b>
<b>D</b>	<b>Appendix D: Tissue compliance results</b>	<b>57</b>
	<b>Bibliography</b>	<b>61</b>

# 1

## Introduction

### 1.1. Background

The motivation of this project arises from the desire to treat coronary artery disease (CAD), a type of cardiovascular disease that is one of the leading causes of death worldwide [1]. CAD is a disease where plaque builds up and hardens in the walls of the coronary artery, narrowing the passage of blood and obstructing the flow of oxygen to the heart. Symptoms include chest pain, shortness of breath, heart attack and even cardiac death [2]. Modern medicine suggests a number of treatment options: lifestyle changes, medical treatment, coronary intervention and coronary artery bypass grafting (CABG), also known as bypass surgery [3]. These treatment options are used separately or combined according to the situation.

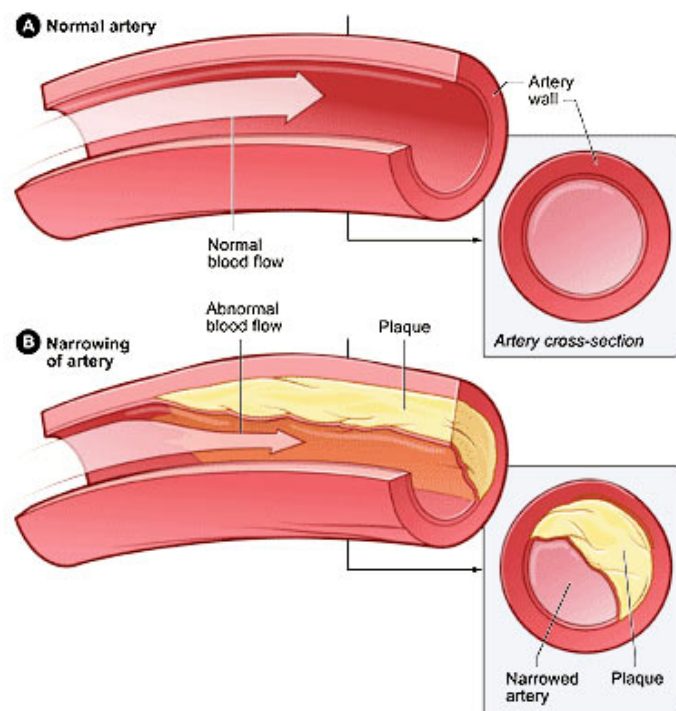


Figure 1.1: Artery blockage is caused due to the inner walls thickening and hardening causing the blood flow to the heart to slow down or cut off completely, which affects the supply of oxygen and nutrients to the heart [4].

The focus of this study is when CAD leads to complete blockage of the artery, which is referred to as occlusion. One of the most challenging types of occlusion is when plaque builds up over an extended

period of time (more than 3 months) and narrows the artery cross-sectional area by more than 99%. This condition is called chronic total occlusion (CTO) [5]. The occlusion builds up over time where it is calcified, causing it to harden. According to Ge, the extent of severity of calcification increases with occlusion duration [6]. The most calcified regions are at the edges, referred to as proximal and distal caps, which are made of hard fibrous material. The proximal cap is reached when the CTO is approached from the antegrade side, which is the reason why it is more thick than the distal cap that is on the retrograde side.

Treating CTOs can be a challenging task and the method depends on various biomedical factors. The treating method explored in this project is called percutaneous coronary intervention (PCI). This is a non-surgical procedure where a cardiac catheter tube is inserted into the coronary arteries in order to improve the blood flow to the heart [7].

The reason why PCI is studied is because it proves quite promising and is preferable over bypass surgery due to shorter hospital stay, reduced hospitalisation costs and faster patient recovery. However, it cannot be concluded which method of the two is more effective, assuming effectiveness entails success rate, postoperative recovery and prevention of disease recurrence after treatment. One of the major drawbacks of PCI is that it is not suited for medically complex cases, which makes it suitable for a limited amount of patients only. Nevertheless, a lot of academic research has been conducted due to its high potential.

Cardiac catheters exist in many types for different functions like stent deposition, intravascular ultrasound for medical imaging, echo-cardiography, pressure/ temperature measurement, use of laser and clot removal or grinding. For the last usage, a catheter is usually inserted to the blood vessel and guided into the heart by the physician. This is done through the groin or arm, as shown in figure 1.2.

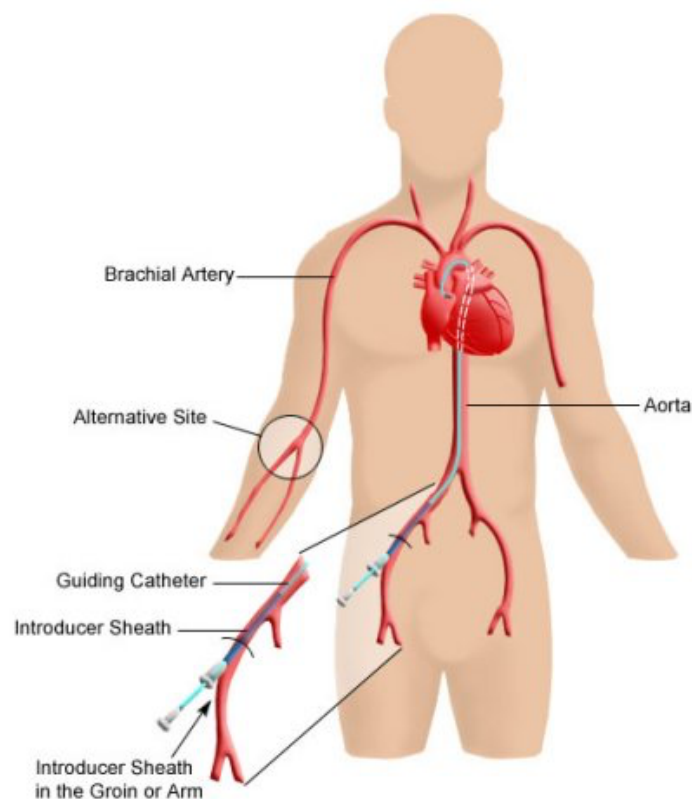


Figure 1.2: Cardiac catheterisation approach through the groin or arm. Through the catheter, a doctor can perform diagnostic tests and treatments on the heart [8].

A method of treating CTOs is by inserting a guidewire through the catheter and penetrating the occlusion

before placing a stent to help keep the artery open. Inflatable balloon tips are also used [7]. However, the success rate of such a procedure is estimated between 55% and 90% [9]. The reason for this is due to the limitation of current PCI techniques, which include guidewire buckling, operator experience and limited instrument output force. Figure 1.3 demonstrates the mechanical solution for PCI and its failure to cross the CTO due to buckling.

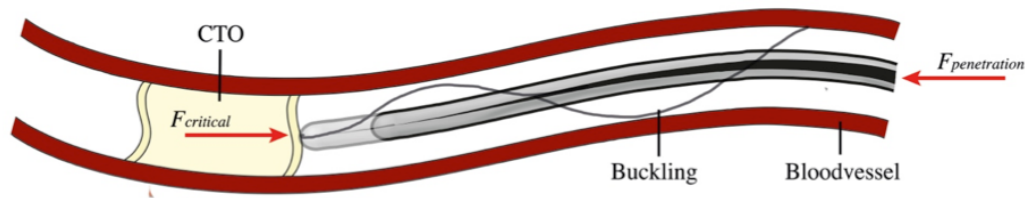


Figure 1.3: Mechanical based solution for treating CTO using PCI. A guidewire is inserted into the vascular system until it reaches the CTO and a static load is applied by the physician to cross it. Guidewire buckling is illustrated, which is a major limitation of the success rate of such techniques [10].

In order to account for these limitations, a cardiac catheter of a different working principle is being developed and studied for its feasibility. This medical device uses hydraulic pressure waves to transfer the energy from the input side to the output tip and successfully penetrate through the calcified CTO cap. In this way buckling is not an issue as there is no solid guidewire involved and the output force can achieve the required values if the device is properly designed. The pressure wave is created by impacting a plunger or piston at the input side, which displaces the liquid inside the tube and causes a compressed region. This compressed region travels longitudinally as a pressure wave and actuates a plunger at the tip of the instrument. As long as the output plunger is already in contact with the occlusion, the energy is transferred directly to the CTO to achieve fragmentation. This concept is illustrated in figure 1.4.

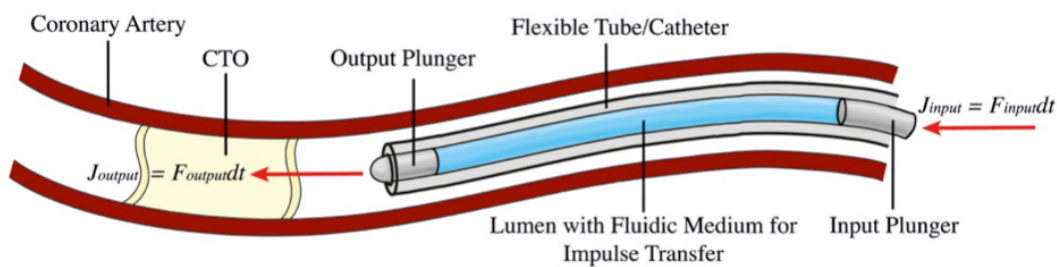


Figure 1.4: Hydraulic based solution for treating CTO using PCI. In this concept a dynamic impulse is exerted on the input plunger of the device, which is converted into translational momentum of the plunger and medium and in turn converted into an output impulse to be exerted to the CTO. Buckling is not an issue any more [10].

## 1.2. Aim & Objectives

As mentioned, coronary artery disease is a major cause of death worldwide which calls for an innovative breakthrough in its treatment options. PCI techniques have a lot of potential due to their lower costs and quicker patient recovery. With the proposed concept, PCI using hydraulic means renders itself more reliable than current state-of-the-art catheter technology as buckling is not an issue anymore. Moreover, with the appropriate design the output force can be adjusted accordingly.

The hydraulic technology exists and a feasibility study has already been conducted by Nicolai [11] on the impulse transfer efficiency, impact method, catheter curvature and catheter elasticity. However, the studies until now have not taken into full account a real situation and no study has been conducted in humans *in vivo*. The feasibility of the device needs to be evaluated by modelling a real situation *ex vivo* first and all the design considerations for a prototype will follow after this. It is thus crucial to study the efficiency of the device in conjunction with the biomechanical properties of CTOs.

In addition to a realistic model, it is also worth exploring the device in terms of its sensing capabilities; the procedure of inserting an external device into the human body might prove useful in providing information otherwise difficult to acquire. Thus, in this project it is also explored if and how it is possible to make the device “smart” and sense certain properties that can be essential for treating the patient or for other diagnostic purposes.

Before diving into all of this, a starting point must be realised. The idea is still in research stage, so a setup made out of simple components and with a common cardiac catheter is to be exploited. The existing setup aims to test the feasibility of the device for a proof-of-concept, so studies have already been conducted with some relevant results which prove useful for further research. On top of that, the existing setup is to be augmented and improved in any necessary way in order to produce a fully operational prototype.

The goal of this study is to realise a prototype device for the treatment of CTO able to operate in two modes: diagnostic and treating. In order to achieve this, certain objectives must be set:

- Explore and understand the existing proof-of-concept setup made by Nicolai [11]
- Implement improvements to the functionality of the setup
- Conduct an *ex vivo* feasibility study where a realistic situation is modelled
- Explore the sensing capabilities of the device for its diagnostic operation mode

### 1.3. Thesis outline

The outline of this report is based on the objectives set to achieve the goal, each objective comprising a chapter on its own. Chapter 2 describes the sources and the background research done prior to and during the project. Chapter 3 is about the existing setup, its main components and how they are understood. Chapter 4 describes and justifies the implementation of the improvements on the existing setup. Chapter 5 goes into the modelling of a real situation and all the main findings from these experiments. Chapter 6 explores the sensing capabilities of the device and presents the experiments done for determining the output target compliance. Finally chapter 7 concludes this report and suggests recommendations for future research.

# 2

## Literature Review

### 2.1. PCI State-of-the-Art

General information on coronary artery disease, chronic total occlusion and their treatment options has been retrieved from the US Heart, Lung and Blood Institute [2], the World Health Organisation [1], the works of Zidar et al. [5], Ge [6] and the book by Jameson et al. with title "*Harrison's principles of internal medicine*" [3]. The current knowledge on state-of-the-art PCI treatment has been explored through four academic sources as well as the US Heart, Lung and Blood Institute [7]. The main research contributions were acquired from the works of Stone et al. [9], Brilakis et al. [12], Osnabrugge et al. [13] and Udaya Prashant [14] concerning the technical approach of PCI, its outcomes, the novel devices used, selection of the appropriate catheter and its cost-effectiveness compared to bypass grafting. The most common PCI procedure is depicted below.

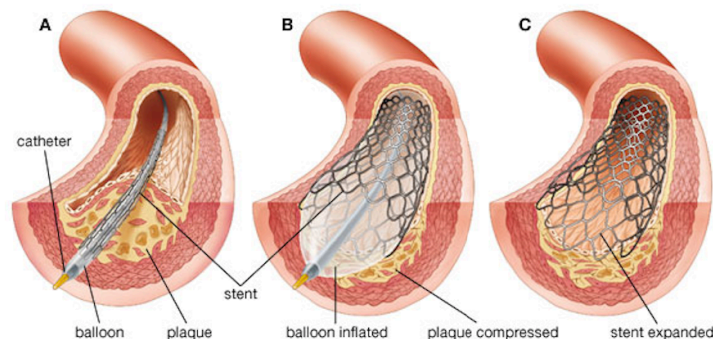


Figure 2.1: **A:** The occlusion is reached and crossed by a cardiac catheter encased in an inflatable balloon and wire-mesh stent; **B:** The balloon is inflated, thus expanding the stent, dilating the artery and compressing the plaque; **C:** The balloon is deflated and withdrawn with the catheter, leaving the stent expanded against the arterial wall [15].

As shown in figure 2.1, the catheter needs to cross the occlusion before inflating the balloon, meaning that the catheter must be inserted into the lesion. This technique does not always result in effectively crossing the occlusion due to buckling of the catheter. As a result, more advanced techniques are being currently developed. State-of-the-art devices of such techniques use high frequency mechanical vibration like the *Crosser* (BARD Peripheral Vascular Inc., Tempe, Arizona, USA) (figure 2.2), blunt micro-dissection like the *Frontrunner XP* (Cordis Corporation, Fremont, California, USA) (figure 2.3) or a rotating drill like the *Kittykat* (Avinger, Redwood City, California, USA) (figure 2.4). All these devices are used for CTO recanalisation<sup>1</sup>.

<sup>1</sup>The process of restoring an interrupted channel of a bodily tube (e.g. blood vessel) [16]

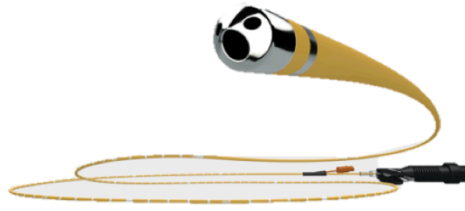


Figure 2.2: Crosser® CTO Recanalisation Catheter. It facilitates central lumen CTO recanalisation via atherectomy and utilises high frequency mechanical vibrations [17].



Figure 2.3: Frontrunner® XP CTO Catheter. It enables controlled crossing of CTO using blunt micro-dissection to create a channel through the occlusion to facilitate wire placement. The actuating jaws open to 2.3 mm and catheter maneuverability is enhanced by the shapeable distal tip and the effective torque control [18].



Figure 2.4: Kittycat2® endovascular catheter. The rotating distal tip helps to minimise static friction during advancement and direct the tip into the lesion [19].

The introduction of new CTO recanalisation technologies like the ones mentioned above has increased the success rate of such interventions up to 90% in experienced hands [20]. This is an encouraging factor for extended research on new concepts for CTO recanalisation. One such concept is the hydraulic pressure wave catheter depicted in figure 1.4. The comparison and possible advantageous outcome of crossing total occlusions by exerting an impulse instead of a guidewire was studied in the work of Sakes et al. "Endovascular Crossing of Chronic Total Occlusions Using an Impulse: An Explorative Design Study" [21]. This article provided useful and relevant information for this concept in terms of the output tip design, actuation method, appropriate dimensions, setup considerations and other relevant factors. Furthermore, the thesis work of Nicolai [11] was used as a reference for the starting point of this study as the feasibility of the device had already been evaluated in terms of its impulse and force efficiency, impacting method, catheter curvature and catheter elasticity.

## 2.2. Hydraulic pressure waves

The main theoretical background to understand the concept involved the propagation of pressure waves through a liquid medium in elastic tubes, which was studied in the book *Applied Hydraulic Transients* by Chaudhry [22] and through the work of Tijsseling and Anderson [23]. The pressure waves are essentially longitudinal waves traveling at the speed of sound. According to Halliwell, the speed of sound  $c$  of a compressible fluid contained in an elastic cylindrical pipe of circular cross section is given by the following equation [22]:

$$c = \sqrt{\frac{K}{\rho \left[ 1 + \left( \frac{K}{E} \right) \psi \right]}} \quad (2.1)$$

where  $K$  is the bulk modulus of the fluid [Pa],  $\rho$  is the fluid density [kg/m<sup>3</sup>],  $E$  is the Young's modulus of the pipe wall [Pa] and  $\psi$  is a non-dimensional parameter defined as:

$$\psi = \frac{D}{e} (1 - \nu^2)$$

where  $D$  is the outer diameter of the pipe [m],  $e$  is the wall thickness [m] and  $\nu$  is the Poisson's ratio of the pipe wall material. For a pipe which is the size of an interventional catheter used for these applications ( $D = 2$  mm and  $e = 0.2$  mm), the relationship between the speed of sound and its elasticity is plotted below:

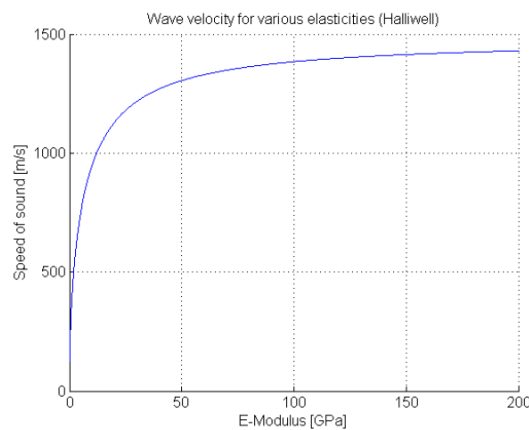


Figure 2.5: Plot of Halliwell equation showing the variation of speed of sound in water with elastic modulus of the pipe wall material. The dimensions used correspond to a common interventional catheter [11].

It is important to note from figure 2.5 that for compliant materials like plastic, the speed of sound is more sensitive to the elasticity of the pipe wall than for hard materials like metals. This means that the choice of the tube material is important. Interventional catheters need to be elastic enough to follow the tortuous vascular system of the patient but for hydraulic pressure wave applications we also need a stiff enough material so that it does not absorb the energy of the pressure wave. At low elasticities, the material selection is particularly important as it makes a big difference in terms of sound wave velocity.

### 2.3. Contact mechanics

Studying contact mechanics and rigid body collisions was also an important aspect of the project, as the input plunger is actuated by an impacting load cell surface. Research was conducted through the works of Chatterjee [24], Paire and Widnall [25] and sources on Hertzian contact theory by Forney [26] and Hanaor et al. [27]. The purpose was to understand the impulse exerted to the input piston and how to optimise it for this application. The main findings are summarised below:

In a rigid body collision, the contact force can be theoretically calculated without the help of computer aided software simulation as long as there is a single point contact. This can be achieved by a sphere-to-sphere or a sphere-to-plane configuration.



(a) Sphere-to-sphere contact

(b) Sphere-to-plane contact

Figure 2.6: The only possible configurations for single point contact. Note that in this context sphere means a 3D spheroid of any curvature, not just spherical.

The equation for calculating the contact force  $F$  is given by [27]:

$$F = \frac{4}{3}E^*R^{1/2}d^{3/2} \quad (2.2)$$

where

$$\frac{1}{E^*} = \frac{1 - \nu_1^2}{E_1} + \frac{1 - \nu_2^2}{E_2}$$

and

$$\frac{1}{R} = \frac{1}{R_1} + \frac{1}{R_2}$$

$E$  is used for the Young's modulus of the material,  $R$  for the radius of curvature of the surface and  $d$  is the indentation depth. The impulse caused by the force  $F$  is defined as the integral of this force over the time  $t$  while it is acting:

$$J = \int_{t_1}^{t_2} F dt \quad (2.3)$$

For a single-point contact, the force-time graph of such an impulse is a bell shaped curve whose dimensions depend on the curvature of the contacting surfaces, their elastic moduli and their total indentation depth. An ideal impulse would have infinite force and zero time duration.

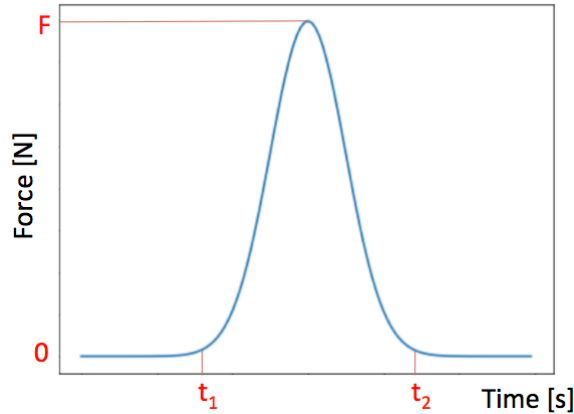


Figure 2.7: Force-time graph of a single point contact. The force acts for a time  $\Delta t = t_2 - t_1$  and reaches a peak value  $F$  at the mid point. The impulse  $J$  is defined as the integral of the force-time graph

## 2.4. Load cell model

The load cells used in this project are strain gauge load cells, which are mechanical elements of which the force is being sensed by the deformation of strain gauges on the element [28]. The strain gauges change their resistance value when deformed.

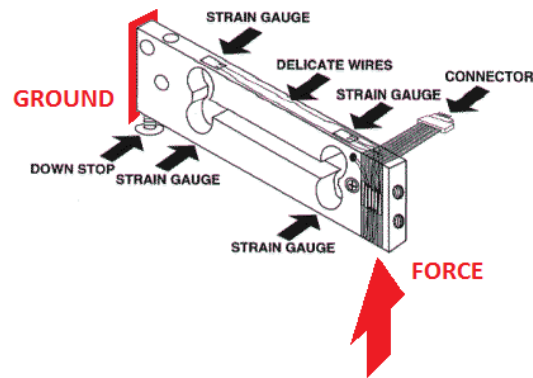


Figure 2.8: A force is applied vertically on the right edge, causing the rightmost strain gauges to deform more than the leftmost, giving an indication of the force magnitude by their difference in resistance [29].

Figure 2.8 shows the common internal components of a load cell. The most important thing to note is that a flexible cantilever-like structure is used with two strain gauges mounted close to the ground/ base (no deformation) and two load cells at its edge (deformed when force is applied, one is compressed and the other is stretched). The cantilever structure suggests there is a stiffness present in the system which connects two masses: half of the cantilever mass attached to the reference ground and the other half suspended. Figure 2.8 depicts a bar load cell but there are many different types of structures depending on the application. The S-type load cell is used for tension and compression measurements and the force can be applied at the middle instead of the edge of the structure, as shown in figure 2.9. A simple mass-spring model of the load cell is depicted in figure 2.10.



Figure 2.9: S-type load cell. If the strain gauges are glued at appropriate locations, this structure is suitable for exerting the force at the middle [30].

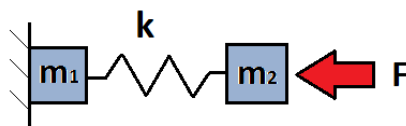


Figure 2.10: Proposed simplistic model of the load cell. For an S-type load cell, the spring stiffness  $k$  of the model corresponds to the top and bottom cantilever bending stiffness and the mass of the S-shaped structure is divided in the two mass components of the model  $m_1$  and  $m_2$ .

The mass-spring model of figure 2.10 suggests that load cells can exhibit resonance when dynamically excited. This is called "ringing effect" and might be an undesired characteristic when measuring force. This model forms the basis in order to study this effect further.

## 2.5. CTO properties

Studies on the nature of CTOs and their biomechanical properties gave reference on how to model an occlusion and what forces to expect in order to cross them. Also, what are the most relevant parts of an occlusion and where is it located relative to the artery lumen were explored through the works of Stone et al. [31], Sakes et al. [21], the book by Yalonetsky et al. "Chronic Total Occlusions. A Guide to Recanalization" [32] and the book by Houwink and De Decker "Elasticity, plasticity and structure of matter" [33], where values for cardiac muscle tissue compliance were obtained and fracture modes of ductile, brittle, soft and hard materials were studied.

Finally, Thind et al. [34] provided a method to determine the proximal cap puncture force needed in CTOs through "A novel method for the measurement of proximal fibrous cap puncture force in chronic total occlusions: the effect of increasing age". This novel method was tested on 44 rabbit femoral arteries and gave a reference for the experiments done as part of modelling the real situation. More specifically, the puncture force mean values at 2, 6, 12 and 15 weeks after the CTO is formed were measured as 0.61 N, 0.78 N, 1.21 N and 1.52 N respectively.

# 3

## Existing Setup

The existing setup is made out of a catheter tube, an impulse mechanism, two load cells, two pistons and two cylinders. Additionally, Thorlabs components and other custom made parts are used. Below are figures depicting a schematic diagram as well as the actual setup.

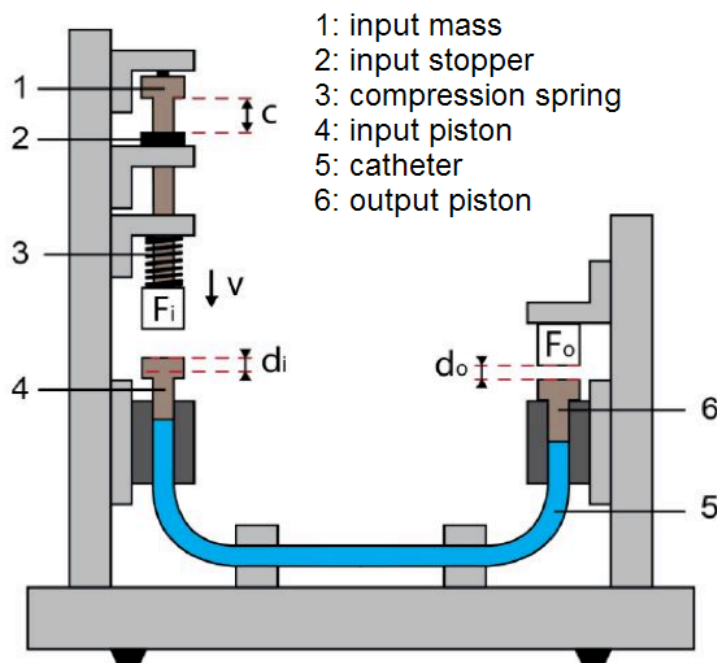


Figure 3.1: Schematic of the existing test facility.  $c$  = spring compression;  $v$  = input speed;  $d_i$  = input piston stroke;  $d_o$  = output piston stroke;  $F_i$  = input load cell force;  $F_o$  = output load cell force.

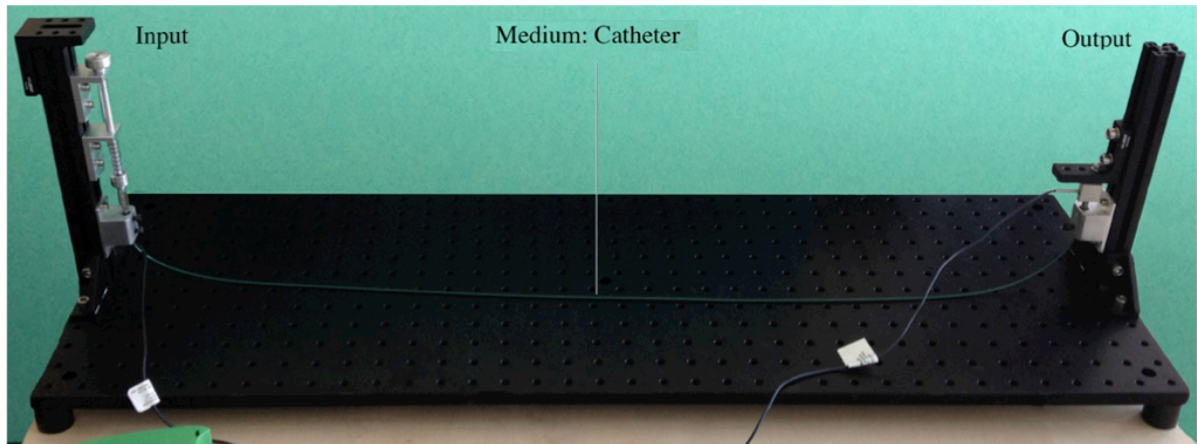


Figure 3.2: The existing setup. A base and parts by THORLABS ® are used to keep the catheter tube, cylinders, actuation mechanism and load cells in place.

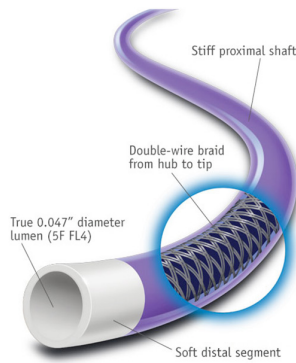
The main components of the setup are described analytically in the following subsections.

### 3.1. Hydraulic catheter

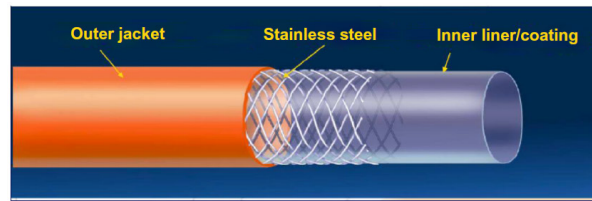
Catheters are used for various biomedical applications, which means there is a wide range for selecting the appropriate catheter for each condition. For this specific application, the basic requirement is that the tube should transfer the pressure wave through a fluid medium with minimal energy losses, as well as being flexible enough to take the unique shape of the tortuous vascular system of each patient. An appropriate model is the Impulse 6F diagnostic catheter (Boston Scientific, Marlborough, Massachusetts, USA) of outer diameter 2.1 mm and wall thickness 0.35 mm. These dimensions are appropriate as the smallest artery that needs to be crossed to reach the CTO is the Right Coronary Artery, which has a minimum diameter of 2.2 mm [35].

At impact the piston generates a high pressure region at one end of the system, which travels along the catheter. This pressure cannot be measured due to the lack of a pressure sensing system but can be estimated by dividing the peak force measured by the impacting load cell over the inner tube area. This results in a pressure of around 15 MPa for an input force of 35 N (see section 5.6 table 5.3 for the required puncturing force). As a consequence of that, a new requirement arises where the catheter tube should be stiff enough so that it does not absorb much energy due to its elasticity. However, this requirement clashes with the desire to have an elastic tube that is able to follow the tortuous vascular system. From the work of Nicolai [11], a COMSOL simulation revealed that the pressure wave magnitude can have a significant effect on the pressure loss. For high pressures of the order of 10 MPa, the effect can cause the pressure to decrease by half in 10 ms according to the simulation. This is a very short time considering that the pressure wave needs around 2.0 ms to travel from the input to the output side (see section 5) which means that an estimated 10% of pressure will be lost from input to output using linear interpolation. In fact the relation exhibits a logarithmic trend, which makes the pressure loss even more (around 15% using the logarithmic fitted curve from the simulation  $y = 7.9 - 1.5\ln(x)$ , where  $y$  is the pressure in MPa,  $x$  is the time in ms and an initial pressure of 7.9 MPa was provided).

The reason why the Impulse 6F was chosen is due to its high enough elasticity to follow the vascular path (Young's modulus is not provided by the manufacturer but the catheter is proven to be suitable for this specific application as it is used on the same vascular path for diagnostic purposes) and uses double wire braiding to counteract the pressure loss effect by stiffening its structure. The catheter and its inner layers are depicted in detail below:



(a) Impulse 6F diagnostic catheter [36].



(b) Catheter layers [14].

Figure 3.3: Structure of catheter tube.

As shown in figure 3.3b, the tube consists of three layers. The outer layer is a soft nylon elastomer jacket which provides flexibility and support to the catheter. The inner layer consists of polytetrafluoroethylene (PTFE). The middle layer in between is a double-wired stainless steel braid which stiffens the catheter to provide strength, kink resistance and allows for easy torquing [14]. For the proof-of-concept experiments, water was used as the liquid medium but in a real situation saline solution would be a better alternative in case of leakage. The physical properties of water can be considered the same as of saline solution, which makes the use of water an acceptable modification.

The length of the catheter tube is 0.9 m. The catheter was cut at the edges and glued to a stainless steel cylinder at each end. The cylinders were manufactured for the piston retrogression with appropriate tolerances. The cylinders are 25 mm long, 5 mm in outer diameter and 2 mm in inner diameter. The pistons are 2 mm in diameter and 17 mm in length, with a piston head on top of that of 5 mm diameter and 5 mm in length.

## 3.2. Impulse

### 3.2.1. Ideal vs real impulse

An impulse  $J$  is the integral of a force  $F$  over the time interval  $t$  while it is acting. It is a widely used engineering tool to excite a system to its natural frequency. An ideal impulse would require a force magnitude of infinity and a time duration of zero, the reason being that such a shape includes the whole frequency spectrum at the same magnitude when decomposed to its harmonic frequencies. Of course this cannot be the case in practice, but a realistic situation can be approximated when a high enough ratio of force magnitude to time duration (for instance 1000 N/s or more) is achieved. The graphical dimensions of an impulse depend on the contact type (e.g. single or multiple contacting points, spherical or flat contacting surfaces) and the material of both surfaces. As explained in section 2.3 in the literature review, for a single point contact we expect a bell shaped force-time graph. The peak force dependence on the surface materials and geometry is explained in the following subsection.

### 3.2.2. Contacting surfaces

The Hertz contact theory predicts that for a sphere of radius  $R$ , elastic modulus  $E_1$  and Poisson's ratio  $\nu_1$  coming in contact with a flat surface (half-space) of material properties  $E_2$  and  $\nu_2$ , the force  $F$  between them is given by equation 2.2, as explained in section 2.3 of the literature review:

$$F = \frac{4}{3} E^* R^{1/2} d^{3/2}$$

where

$$\frac{1}{E^*} = \frac{1 - \nu_1^2}{E_1} + \frac{1 - \nu_2^2}{E_2}$$

and  $d$  is the indentation depth. The force-time graph is a bell-shaped curve in theory which reaches a peak force  $F$  at its mid-point. Since a finite energy is given to the sphere to strike on the surface, a finite

impulse will be given as well in the time interval between  $t_1$  and  $t_2$  when the force is acting, expressed as  $J = \int_{t_1}^{t_2} F dt$ . This means that the area under the force-time graph is limited by the energy provided. Having a higher force means we have a shorter time duration, which resembles an ideal impulse more closely. Equation 2.2 implies that the higher the elastic moduli of the two contacting surfaces, the higher the force.

### 3.2.3. Impulse measurement by load cell

An experimental apparatus was set in order to measure an impulse by the load cell. According to Hertz contact theory, a hard surface needs to hit the load cell at a single-point contact. This can be achieved by a metallic sphere suspended by a pendulum. The pendulum is always retracted by 3 cm, providing a systematic impulse energy. A screw is attached at the load cell so that the contact is confined to a smaller area and multiple contact points are prevented.

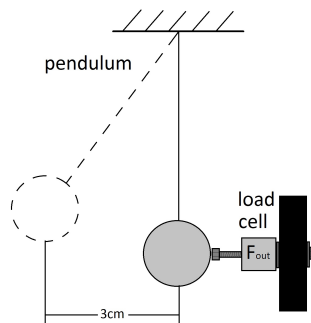


Figure 3.4: Experimental apparatus for measuring impulse. The load cell is tightly bolted onto the breadboard using nuts and bolts. It is then oriented such that its measurement axis is horizontally aligned with the pendulum direction. The sphere is always retracted by 3 cm.

When the sphere is released, the following force is measured by the load cell.

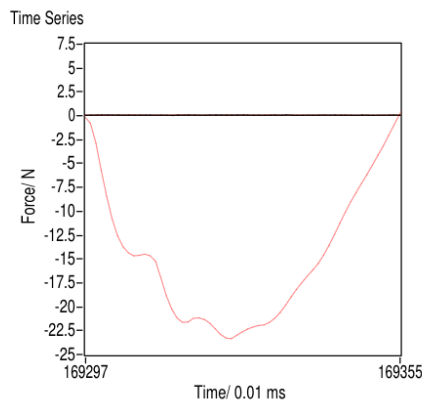


Figure 3.5: Impulse measured by the load cell using the experimental apparatus described. The force magnitude is negative as the load cell convention is negative for compression and positive for tension.

The duration of the impulse is 0.58 ms and its magnitude goes up to 23 N. The area under the curve is computed to be 0.0086 Ns, which in theory is also the momentum of the sphere when it hits the load cell, according to the impulse-momentum theorem. It is apparent that the force-time graph is not a perfect bell-shaped graph as expected from theory. It also exhibits an oscillatory behaviour, which is explained in section 3.3.2.

In conclusion, an ideal impulse cannot be achieved in practice. However, an ideal situation can be approximated by using a single point contact (e.g. spherical-to-flat or spherical-to-spherical surface)

and as stiff material as possible in terms of elastic modulus. Impulses achieved in the lab and measured by the load cell revealed aspect ratios of around 40.000 N/s, producing a force of 23 N in 0.6 ms by impacting a metallic sphere to the load cell attachment, as explained earlier.

### 3.2.4. Impulse mechanism

In order to provide an impulse to the input piston, a simple mechanical actuation method was used. The mechanism consists of a pre-loaded spring in a vertical configuration. A motion limiting mount with a screw act as an adjustable upper limit for the initial position of the spring before being released. In this way, the input momentum can be determined. A rubber stop is also in place to absorb the vibrations from the abrupt stop of the impacting mass. At the impacting edge, the load cell is tightly fixed. This mechanism was designed out of Thorlabs components and custom made parts. The mechanism is depicted in figure 3.6 and it is shown as part of the whole setup in figure 3.1. Its dimensions are clearly shown in a schematic representation in appendix A.

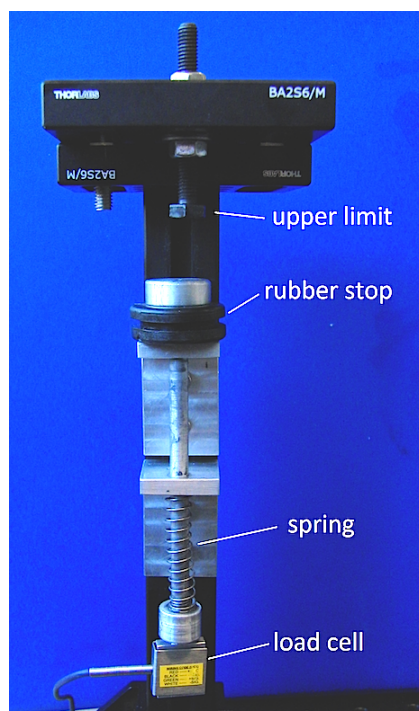


Figure 3.6: Impulse spring mechanism. The mechanism can be pulled upward in a loaded position and then released to impact the piston.

## 3.3. Load cells

### 3.3.1. Sensor type and configuration

Load cells are transducers that convert a mechanical force to an electrical signal. Most load cells use strain gauges as their measuring principle; when a load is applied, the strain gauges deform which causes a change in their electrical resistance. This change can only be measured when an excitation voltage is provided, which renders it an active sensor.

Apart from active, load cells are also analog devices. In order to measure the minute change in resistance of the strain gauges, a Wheatstone bridge configuration is used in the signal conditioning circuit. The differential output signal is then passed through an instrumentation amplifier and then to an Analog-To-Digital Converter (ADC) before being stored and processed in a PC.

Two load cells were used for measuring force, one at the input side and one at the output. The model used was the LSB200 Miniature S Beam series (Futek, Irvine, California, USA) measuring up to 10 lb (44 N). This model has two M3 female threads on the sensitive sides for attachments. The load cell

signal was passed to a CPJ RAIL analog signal conditioner (Scaime, Juvigny, France) and then the data was acquired through the NI USB-6211 DAQ interface (National Instruments, Austin, Texas, USA). The data was then stored and manipulated on a PC using LabVIEW 2014 (National Instruments, Austin, Texas, USA). Through LabVIEW, it was easy to calibrate the sensors and introduce any necessary offset, as well as setting the sample rate and sampling time. The rate was set to its maximum possible value of 100 kHz, sampling for 5 s.



Figure 3.7: Components of the measuring system. The output signal from the load cell is amplified in the signal conditioner and converted into digital form through the DAQ device before being processed and stored in a PC using LABVIEW.

### 3.3.2. Ringing effect

A characteristic feature of load cells is that during and after an impact or any abrupt load change, they keep vibrating at their resonant frequency, referred to as “ringing effect”. This phenomenon occurs as a result of the spring-like characteristics of the internal components of a load cell; usually the strain gauges are attached to a cantilever structure which is free to oscillate at its natural frequency when excited (see section 2.4 in the literature review). The proposed load cell model is depicted in figure 2.10. This effect might cause confusion in future measurements, so it must be understood. The experiment that follows aims to identify this effect.

#### Experiment for identifying sensor ringing

A way of exciting the sensor to its natural frequency is by providing an impulse. This is achieved by a metallic sphere attached on a pendulum, as explained in section 3.2.3 (see figure 3.4). On the sensitive side of the load cell an attachment can be tightened at the female thread. This is very useful, as the contact area of the sensor can be confined to a much smaller size than its flat surface. The benefit of this is that the impacting object will not hit at multiple points on the sensor causing a distorted impulse. This series of experiments aims to study if and how a different type of attachment alters the impulse shape and sensor ringing. There are three types of attachment used: a short bolt of length 1.8 cm, a long bolt of length 3.2 cm and a plastic spherical knob of diameter 1.6 cm and total length of 2.8 cm, all depicted in figure 3.8.

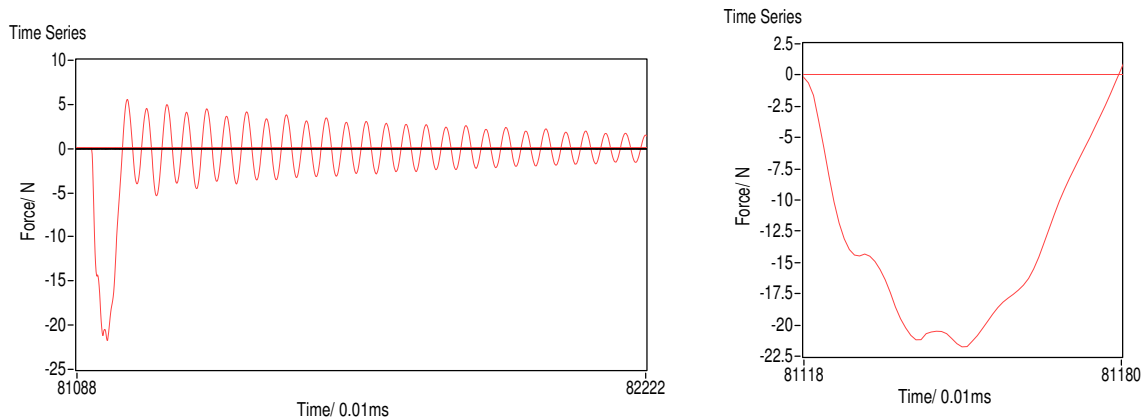


Figure 3.8: The three different sensor attachments used in this experiment: a short bolt, a long bolt and a plastic spherical knob.

## Results and conclusions

The main results of this experiment were confined to a force-time graph acquired by the sensor due to

the impact, as well as a Fast Fourier Transform (FFT) diagram used to identify the dominant frequencies of the oscillating system as a result of the ringing effect. The three different attachments produced some interesting differences in the results. The Force-Time graph of the short bolt attachment is shown in figure 3.9. The ringing effect is depicted by the oscillations following the impact (figure 3.9a), as well as during the impact (figure 3.9b).



(a) Ringing effect appears as an oscillating force.

(b) Impulse (zoomed in). The duration is 0.62 ms and the magnitude goes up to 22 N.

Figure 3.9: Force-Time graph for the short bolt attachment.

As mentioned in section 2.4 of the literature review, the proposed simplistic model of the load cell is a double mass-spring system with one mass being attached to a steady reference frame ( $m_1$ ) and the other free to oscillate ( $m_2$ ), as shown in figure ... As a result, it is reasonable that after a dynamic impact the load cell exhibits a resonating behaviour. The resonance of the load cell is apparent in two phases.

After the load cell is excited by the impact, the resonance is clearly visible by a slowly damped oscillation in figure 3.9a. The resonating frequency can be accurately determined by the FFT diagram:

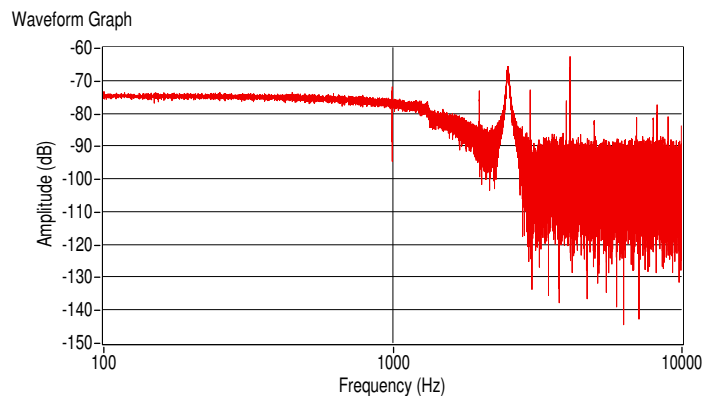
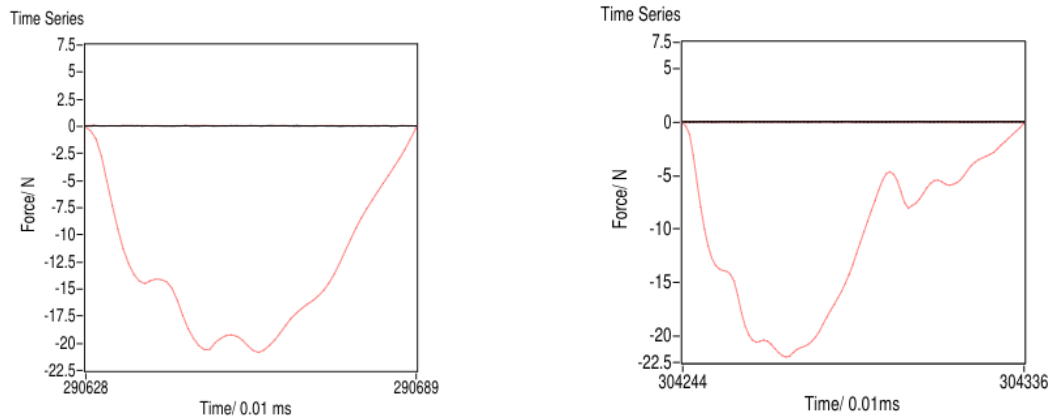


Figure 3.10: FFT graph for short bolt. Peak is clearly visible at 2500 Hz, indicating the ringing effect resonance.

Apart from the resonance after the impact, the load cell seems to resonate during the impulse duration as well. This resonance is superimposed on the impulse shape, which is one of the factors that distorts it from an ideal bell-shaped graph (see figure 3.9b). However the period of this oscillation is not the same as the ringing effect resonance. It is likely that this is another vibrating mode of the structure at a much higher frequency (around 9-10 kHz), that the double mass-spring model does not account for.

After the other two attachments were tested, it was concluded that the attachment type has an effect on the shape of the impulse, shown in the zoomed in Force-Time graphs of figure 3.11. For example,

the long bolt has a much more irregular surface due to its slot. When compared to the short bolt which has a more rounded shape, the impulse shape shows some considerable difference.



(a) Short bolt: Impulse duration = 0.61 ms

(b) Long bolt: Impulse duration = 0.92 ms

Figure 3.11: Impulse sensed by the load cell for the short and long bolt attachment.

The main conclusion of this experiment is that the ringing effect is dependent on the attachment used. For instance, the spherical knob produces a lower resonance at 1710 Hz, the reason being that its higher mass adds up to the mass  $m_2$  shown in the proposed model (figure 2.10) and produces a lower frequency due to their inverse relation. Another remark is that the tighter the attachment is screwed the higher the resonating frequency. This difference is no more than 100 Hz but is identifiable as the FFT peak is repeatable within 10 Hz. A possible reason for this is the backlash of the thread. In addition, the type of attachment has an effect on the impulse shape. The most appropriate attachment to be used from these three is the spherical knob due to its shape (single-point contact). However, a more hard (e.g. metallic) material would be preferable for the final design as the impact momentum would be transferred to a greater extent instead of being absorbed by the material. This would lead to a sharper force-time graph with a higher peak force and a shorter impulse duration.

# 4

## Improvement of Setup

The existing setup was used to design a proof-of-concept which produces some results in terms of the impulse transfer, impact method, catheter elasticity and catheter curvature. In this project only the impulse transfer is of interest. An indication of impulse transfer is the peak force efficiency. As will be shown later, the purpose is to model a real situation and evaluate the treatment performance, as well as to use the device for diagnostic operation. It is therefore crucial to improve and augment the setup in order to achieve a more robust and realistic demonstrator.

### 4.1. Avoiding air entrapment

A major challenge of the current setup is filling the tube with water as fully as possible. A way of doing this is by having the tube in an upright configuration as shown in figure 3.1, where the cylinders and pistons are vertical. After taking out the pistons, water is pumped in the input cylinder via a syringe. Water and air bubbles are forced out from the output cylinder until there is no more air and only water is leaking. This indicates to stop pumping with the syringe and as a result a water dome is formed at the output cylinder. The output piston is inserted after being lubricated, which causes the water to be pushed back and form another dome at the input side. Finally, the input piston is also inserted and the system can be hydraulically actuated.

Unfortunately, air bubbles can be trapped in the tube which introduce further damping to the system and impede the pressure wave motion. The problem with the air entrapment arises when the input piston is impacted. Making use of the High Speed Camera revealed that water splashes out at the input side when the piston is hit, due to its sudden displacement. Also, when the cylinder is not horizontal, the piston falls due to gravity, causing water to be displaced out through the clearance. This is likely to cause air to make its way inside the tube.

A way of solving this issue is by immersing the piston and cylinder into water. This will not guarantee that the system will not loose water, but it can prevent air entrapment. This solution is implemented by means of a water filled container which has a rubber seal at its bottom for the cylinder to be tight and to prevent water from leaking. The idea is depicted below:

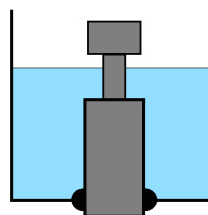


Figure 4.1: Solution implemented for preventing air entrapment in the tube.

This idea was implemented only at the input side. The output was turned horizontal (see section 4.4) to avoid the piston falling due to gravity. It was concluded that the pressure wave speed and transmissibility of the piston motion did not degrade after several attempts. The same was observed for the force transmissibility (both static and dynamic). This suggests that indeed the air from the input side was the cause of the deterioration of the device's performance. A huge advantage of this improvement is that there is no need to refill the tube after every strike.

## 4.2. Load cell attachment

As explained in section 3.3.2, the load cells can accommodate attachments via their M3 female thread. The load cell sensitive surface is a rectangular flat surface that comes in contact with the piston head flat surface. Two impacting flat surfaces means that they come in contact at multiple points, distributing the energy among them. Also, due to difficulty of perfect alignment, different contact points might touch each other at different times. These effects cause a more widespread and lower magnitude force to be sensed by the load cell. As explained in section 3.2.1, a high magnitude force in a short time interval is desired for a realistic impulse. Thus, a single-point contact should be achieved with the appropriate attachment.

A single-point contact can be between two spherical geometries or between a spherical and a flat. One option is to glue a metallic half-sphere on the piston head. Another option is to attach a spherical object to the load cell. This was achieved using a spherical knob. Indeed the impact produced a much more clear impulse, also shown through the FFT diagram which exhibited a more flattened graph towards high frequencies, as an ideal impulse contains all frequencies in theory. One disadvantage of this knob was its material; plastic is able to absorb some of the energy from the impact which should be avoided when designing the real device. A metallic material would be the best option due to its hardness. The load cell with the attachment is shown:



Figure 4.2: Plastic spherical knob attachment tightened to the load cell.

## 4.3. Need for a membrane

The water filled container solved the issue of air entrapment but there were some other problems present: the input piston falling due to gravity was still an undesired phenomenon. In addition, water was splashing out of the container, meaning that after 4 to 7 strikes the container needed refilling to prevent water level of falling below the cylinder clearance height.

Furthermore, when the input piston is hit, it needs to retract to its initial position. The need for this is mostly as a reference for experimental purposes but also to be able to give an impulse to the input piston and return the system to its initial state. These reasons led to the conclusion that some stiffness has to be introduced that will retract the piston to its original position. This stiffness can be estimated by dividing the force required to counteract the weight of the piston by the input piston stroke. For estimating purposes, the values are rounded off. The weight of the piston is almost 0.01 N and the stroke used can be as high as 5 mm. Thus, a stiffness of 2 N/m would be enough in theory. This stiffness can be provided by means of an elastic membrane. The membrane chosen was a common PVC plastic wrap used for sealing food. The choice was made on the basis of its properties, as it is quite resistive to ripping by stretching it and its very low thickness (no more than 10  $\mu\text{m}$ ) gives the desired flexibility for retracting back the piston by exerting a force on its head. The stiffness of the membrane was tested by stretching it and attaching it to the walls of a plastic container before exerting a force by the load cell. The load cell measured the force and the displacement of the membrane was measured by a caliper. The stiffness order of magnitude was estimated to be 10 N/m, at least one order of magnitude higher than the minimum requirement. The function of the membrane is depicted below:

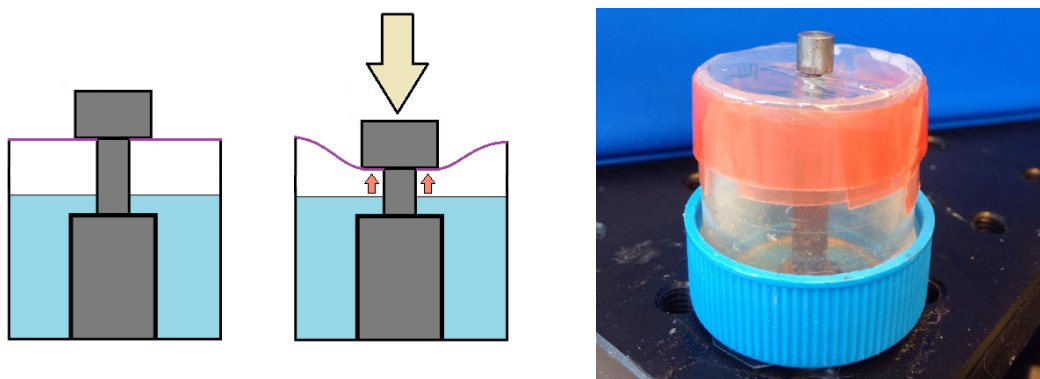


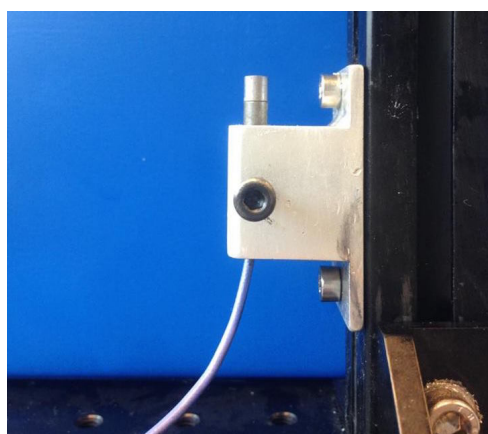
Figure 4.3: Addition of membrane and its function. Tape is used to keep it stretched.

As shown, the membrane acts as an opposing force when the piston moves downwards, either by gravity or due to an external force. It creates a semi-closed system, as it prevents water from splashing out from the input side. It also prevents the piston from falling and retracts it to its initial position.

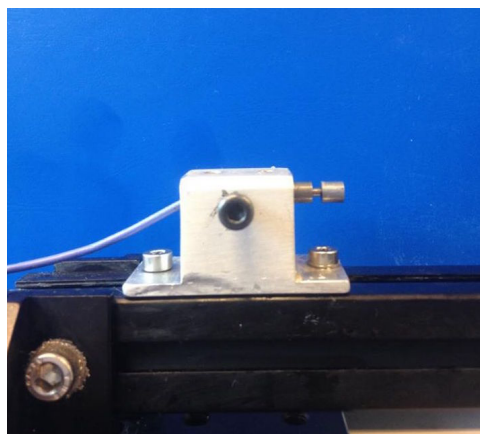
Another benefit of this modification is that when the device was tested for its peak force efficiency (see equation 5.1 and figure 5.2), the membrane produced much less deviated results compared to the non-membrane case. These can be shown in appendix B where the peak force efficiency of the system is measured and the input and output peak forces of the non-membrane case show a higher standard deviation compared to the ones with the membrane. More specifically, the standard deviation of the efficiency without the membrane is 8.7% of the average value, almost double of the case with the membrane, where it is 4.3%.

#### 4.4. Orientation of output

The original orientation of the output was vertical. However, this causes the problem of a falling piston due to gravity, as explained earlier. Rotating the output cylinder to a horizontal orientation prevents the piston from moving at its resting position and no water leakage occurs, as long as the piston stroke is limited to less than 5 mm. It also makes the experiments more realistic, as in a real situation the patient would lie horizontally when the PCI is performed.



(a) Vertical output (existing setup).



(b) Horizontal output (improved setup).

Figure 4.4: Changing the output tip configuration from vertical to horizontal deals with the piston falling due to gravity.

#### 4.5. Adjustable input stroke

Ideally, the pistons should have a motion transmissibility of unity due to their identical area. This means that the output piston is displaced exactly as much as the input piston does. In a real PCI treatment,

complications might occur due to a tortuous vessel or a misplaced output tip. For safety reasons, the output piston stroke should not exceed 2 mm, otherwise there is the risk of damaging the artery walls or other healthy tissues. As a result, the requirement for an adjustable input stroke arises.

The impact mechanism is fixed on the base, so its released position will always be at a specified height. What needs to be adjusted is the initial position of the piston, as it will stop at the same final position anyway. This can be achieved by using a Thorlabs height adjustment mechanism, as shown below:

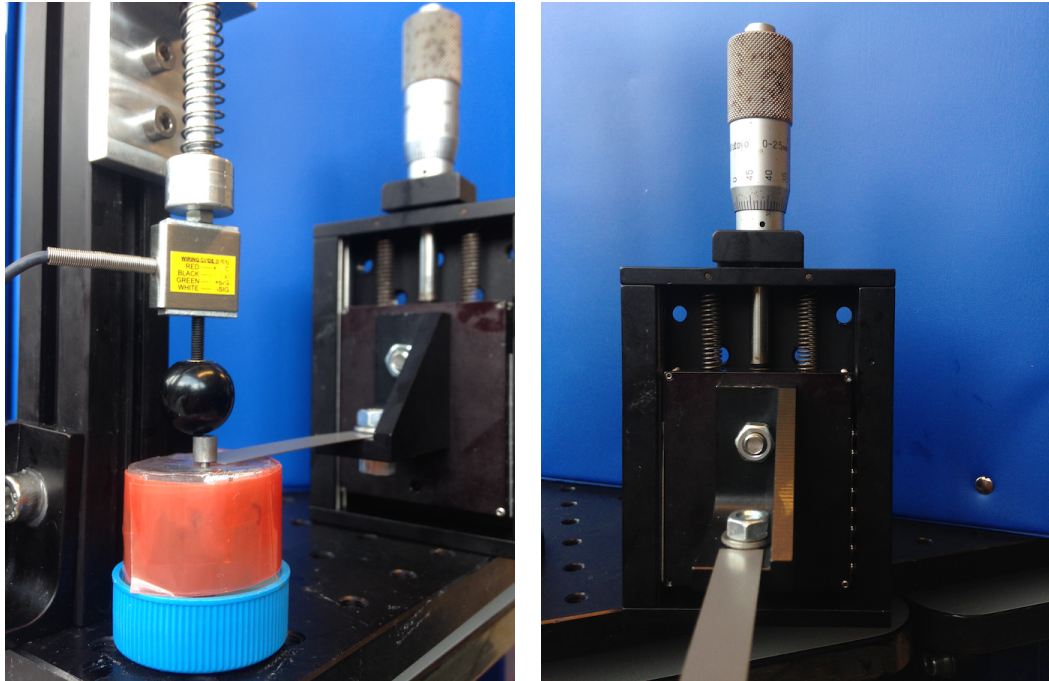


Figure 4.5: Input stroke adjustment mechanism can achieve any stroke desired to micrometer precision.

# 5

## Simulation of the PCI procedure

The improved setup does solve some practical problems but it does not take into consideration a real PCI where the physician pushes the tube against a CTO of certain physical properties. This section aims to replicate a replication of the device and CTO and investigate how the peak force efficiency is affected by four different considerations independently.

In the current setup there are four basic limitations, hindering a realistic representation of the system.

- The output cylinder is fixed in place. In reality the output cylinder of the catheter can slide along the artery path. When the device is triggered, the output piston will launch forward, causing the output cylinder to recoil backward. In addition, there is some resistance to this recoiling motion due to the presence of blood, which impedes the sliding of the tip.
- The output piston hits the rigid metallic surface of the bolt head attached to the load cell. In reality the catheter tip is in contact with the proximal cap of the CTO, which has specific material properties.
- The output load cell, which measures the force felt by the CTO, is fixed in place. In fact the CTO is strongly coupled to the artery walls, which are in turn connected to cardiac muscle tissue of the heart of an estimated Young's modulus between 100 kPa and 130 kPa [21].
- The mass of the load cell and its attached bolt is not the same as the mass of the CTO. This causes a distorting effect on the measurement, since a much lighter object is impacted in reality. Ideally the load cell should have the same mass as the CTO.

All four effects should be taken into consideration when measuring peak force efficiency. The following subsections describe how these deficiencies were tackled and what results were produced. Each step deals with one of the aforementioned points separately in order to determine their effects individually.

### 5.1. Reference setup

Before adding all these considerations, a reference should be taken to be compared with. This reference is the setup after all the improvements of chapter 4 with the membrane and piston stroke adjustment at the input, a horizontal output orientation, a plastic spherical knob attached to the impacting load cell attached at the tip of the impulse spring actuator mechanism.

The variables measured are the input peak force  $F_{in}$ , output peak force  $F_{out}$  and the time needed for the pressure wave to travel from the input load cell to the output load cell  $\Delta t$ . From  $F_{in}$  and  $F_{out}$ , the peak force efficiency  $\eta_p$  is calculated.

$$\eta_p = \frac{F_{out}}{F_{in}} \times 100\% \quad (5.1)$$

The input peak force is the independent variable in the sense that the impacting mechanism is always released from the same position and the stroke adjustment is fixed to a stroke of 4 mm. However, there are still small variations in  $F_{in}$  as the actuation is mechanical and cannot provide a highly consistent force. The dependent variables are  $F_{out}$  and  $\Delta t$ .

The tests were conducted 17 times for each situation, according to the power analysis conducted using the G\*Power software [37] for the required minimum number of repetitions needed. Using a significance level  $p$  of 0.05 and an effect size of 0.4, the minimum number of repetitions turned out to be 15, so 17 was used to minimise the effect of outliers and to be consistent with the relevant work done on this setup previously. Thus, unless stated otherwise, the number of repetitions for each experiment is 17.

In this setup, without simulating the real situation, the output piston is in contact to the rigidly fixed load cell and the output cylinder is also fixed in place by means of a tightened screw as shown in figure 5.1.

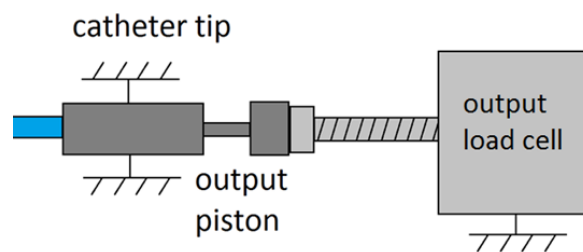


Figure 5.1: Schematic of output tip, piston and load cell without any simulating steps taken.

Typical results from this experiment look similar to figure 5.2.

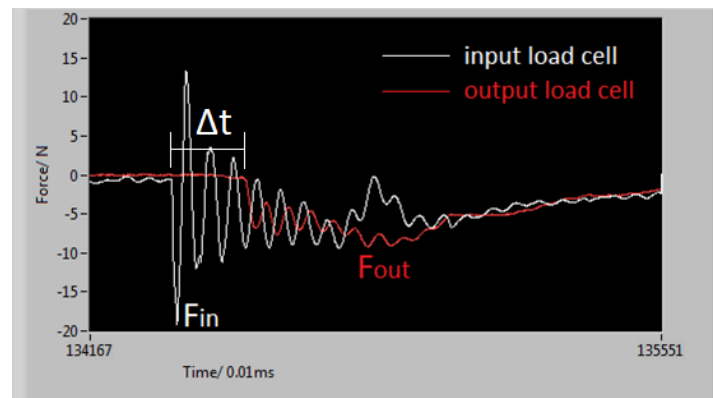


Figure 5.2: Typical results without simulating the real situation.

For the peak forces (input and output), the most extreme values were used. The time interval  $\Delta t$  is the time needed for the signal to travel from one load cell to another. This means that it is not only the travel time of the pressure wave in the tube but also through the other media (piston, contact surface etc.) and is also dependent on factors like the friction of the piston inside the cylinder and the tolerance of the cylinder internal diameter. The results are shown in appendix C table C.1. The values are indicated as *mean ± standard deviation*. For this experiment, the input peak force was measured to be  $F_{in} = 20.5 \text{ N} \pm 1.2 \text{ N}$ , the efficiency  $\eta_p = 50.3\% \pm 2.0\%$  and the pulse travel time  $\Delta t = 1.9 \text{ ms} \pm 0.1 \text{ ms}$ .

## 5.2. Step 1: Sliding of the output tip along the artery wall

### 5.2.1. Simulation

The first simulating step is to enable the motion of the output cylinder along the path of the artery. This is achieved by loosening the screw of the current setup at the output block that holds the cylinder in place. In addition, lubricating oil is inserted in the pathway for better sliding. In fact, the lubrication causes motion of minimal friction, which is not the case in a real situation due to blood surrounding the output tip; blood can cause a considerable resistance to motion. Assuming the recoiling of the cylinder will cause a drop in output force due to its premature detachment from the load cell, the lack of friction creates a worst-case scenario in terms of efficiency and can be indicative for simulating purposes. A schematic of the setup is shown in figure 5.3.

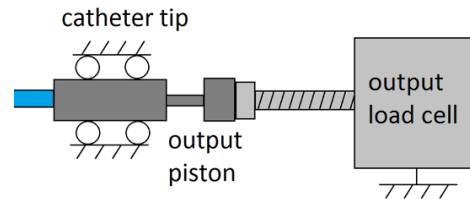


Figure 5.3: Schematic of the setup when sliding of the output tip is taken into account.

### 5.2.2. Results

For this experiment, an input peak force of  $F_{in} = 20.6 \text{ N} \pm 1.1 \text{ N}$  was measured, an efficiency of  $\eta_p = 42.8\% \pm 3.7\%$  and a pulse travel time of  $\Delta t = 2.0 \text{ ms} \pm 0.1 \text{ ms}$ . The results can be found in appendix C table C.2.

### 5.2.3. Conclusions

The contribution of this step is to simulate the sliding motion of the output tip along the artery wall. This produced an 8% reduction in peak force efficiency, a factor of 0.85 of the reference efficiency of the device. The input peak force and pulse travelling time remained the same as without the simulation. This suggests that the recoiling indeed has a deteriorating effect on efficiency and this experiment demonstrates a worst case scenario in terms of friction.

## 5.3. Step 2: Material properties of the CTO proximal cap

### 5.3.1. Simulation

The second simulating consideration involves the contact surface of the output piston. According to Hertzian contact mechanics, the amount of deformation, and thus surface forces, is dependent on the elastic moduli of both contacting surfaces. This means that hitting a rigid metallic surface (bolt head) will produce a higher output force than hitting something more flexible. CTOs are not totally rigid, so the effect of having an elastic surface in contact with the output piston should be investigated. This elasticity is provided by a piece of foam typically used for packaging, which is a soft material that resembles the CTO proximal cap. Of course, it does not have the exact bio-mechanical properties of a CTO, but it can be used for a pilot test before making a more complete and accurate replication.

A foam piece of thickness  $t$  is stuck in between the output piston and output load cell, as shown in figure 5.4. Four foam pieces of different thickness were used so that the effect of a varying thickness is investigated. When the foam is cut, there is a considerable amount of uncertainty in thickness due to its irregular surface, which is shown as an error in the graph of figure 5.4. The load cell is just behind the foam piece, so it measures a damped force which by analogy would be the force transmitted all the way to the back side of the proximal CTO cap.

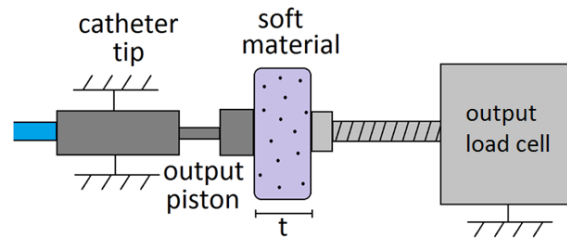


Figure 5.4: Schematic of the setup when a compliant contact surface is taken into account.

### 5.3.2. Results

The results for the peak force efficiency for different foam thicknesses are plotted in figure 5.5. Each data point represents the average value from the 17 repetitions and the vertical error bar represents the standard deviation. The horizontal error bar is the uncertainty of the foam thickness and its value is 1.0 mm for all data points due to the irregular foam surface. The first data point at  $t = 0$  represents the unsimulated situation described in section 5.1, where the piston is in direct contact with the bolt head of the load cell. The full results are summarised in appendix C tables C.3, C.4, C.5 and C.6.

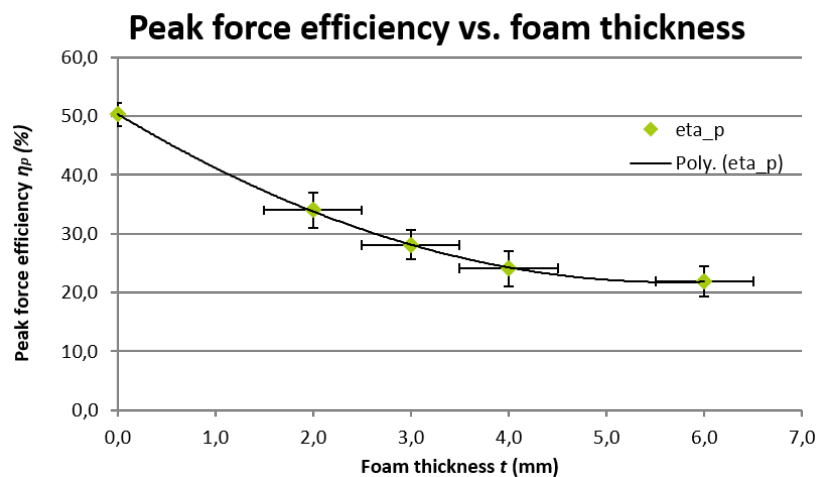


Figure 5.5: Plotted graph of peak force efficiency  $\eta_p$  for different foam thicknesses  $t$ .

Regarding the input peak force, there has been a slight decrease (see appendix) by 0.5 N on average from all four non-zero thickness data points. The travel time of the pressure wave  $\Delta t$  has also changed slightly to  $2.3 \text{ ms} \pm 0.1 \text{ ms}$ .

### 5.3.3. Conclusions

The goal of this step is to simulate the CTO material using foam. This produced a decrease in efficiency as expected; the efficiency is falling with a decreasing rate as the thickness of the foam increases. It is worth noting that the horizontal error bars do not have a significant effect on the fitted curve. This means that the surface irregularities did not have a significant effect on the measurement, as the average thickness of the foam was of importance. The reducing trend in efficiency seems to level off after thickness values of 4 mm. The thickness of a CTO proximal cap is around 0.5 m which, according to the graph of figure 5.5, corresponds to an efficiency of 46%, a factor of 0.92 of the reference efficiency.

Regarding the input peak force  $F_{in}$ , it is suggested that the slight drop is caused due to the change in the compliance of the system as a whole. The compliant parts of the system comprise of the input piston, water, tube, output piston and the contact of the output piston. Since the contact of the output piston is now changed to something more compliant, it is reasonable that the input peak force reduced as the whole system is less stiff and can be displaced more.

The pressure wave travel time  $\Delta t$  also appeared to have changed by an increase of 0.3 ms. As mentioned before,  $\Delta t$  is the time needed for the transmission of the wave energy through all the media, including the pistons and their contact surfaces. Since there is some more material added between the output piston and the load cell, the travel time increases as the wave has to travel through a longer distance.

## 5.4. Step 3: Connection of the CTO to the heart tissue

### 5.4.1. Simulation

The third step aims to investigate the effect of the CTO coupling to a flexible heart tissue. As stated earlier, the CTO is strongly connected to the artery walls, which in turn are connected to heart tissue. The simplest way of simulating flexibility is by using a spring. The spring should be attached between the CTO and the fixed world. The best method of doing this is by attaching a spring at its back, as shown in the schematic of figure 5.6.

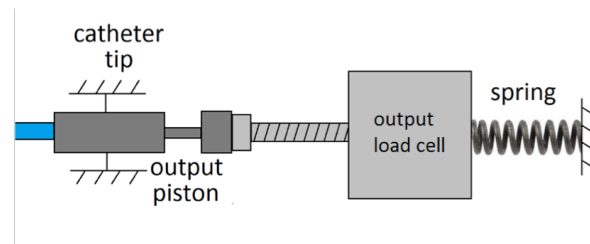


Figure 5.6: Schematic of the setup when the connection of the CTO to the heart tissue is taken into account. The connection is modelled by a spring.

The spring used (ALCOMEX D1680) has a stiffness of 2.67 N/mm (indicated by the manufacturer) which does not necessarily coincide with the flexibility of heart tissue. However, for indicative purposes it can show the trend since it is a quite stiff spring and the transition from the no spring situation is not so abrupt.

### 5.4.2. Results

In this situation the peak force efficiency was measured to be  $\eta_p = 24.2\% \pm 4.4\%$ , the input peak force as  $F_{in} = 19.1 \text{ N} \pm 1.6 \text{ N}$  and the pressure wave travel time as  $\Delta t = 2.0 \text{ ms} \pm 0.1 \text{ ms}$ . The results are summarised in table C.7 in the appendix.

### 5.4.3. Conclusions

The aim of this step is to simulate the coupling of the CTO to the artery walls by suspending the load cell by a spring instead of having it rigidly fixed. This caused a drop in efficiency by half, indicating that even with a stiff spring the effect is quite immense. The input peak force also dropped by 1 N compared to the reference unsimulated situation, owing to the more compliant system, as explained before. The pulse traveling time is unchanged, as there is nothing added in between the load cells to slow it down.

### 5.4.4. Step 3 with pre-load

It is worth investigating what happens when a pre-load is applied to the spring before the impact. The pre-loaded situation corresponds to the catheter being pushed against the CTO by the physician before puncturing. The pre-load was achieved by tightening the load cell at another position where the attached spring is compressed, providing a constant force to the load cell. This means that the output piston is now at its closed position, as shown in figure 5.7.

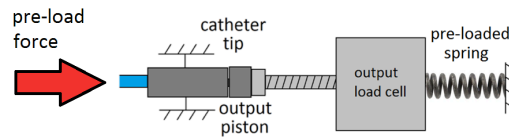


Figure 5.7: Schematic of the setup when the pre-load applied by the physician is taken into account. This is simulated as a static force compressing the spring.

The pre-loading force was kept to 0.6 N as too much pre-load caused water to leak out from the output cylinder at impact. The efficiency appeared to slightly increase to  $\eta_p = 26.4\% \pm 2.3\%$ , owing to the already compressed load cell which measures the output force on top of the pre-load force.

The input peak force was observed to increase to the reference values again of  $F_{in} = 20.7 \text{ N} \pm 1.3 \text{ N}$  due to the pre-load which creates a stiffer connection. This means the load cell will not move as much as in the non pre-loaded case and the input load cell will sense a higher stiffness. The results are summarised in table C.8 in the appendix.

## 5.5. Step 4: Mass of the CTO

### 5.5.1. Simulation

The final simulating step takes into consideration the actual mass of the CTO. In an ideal scenario, the load cell, which measures the force exerted on the CTO, should have the same inertia as the CTO. The load cell with the bolt attachment weighs 7.2 g and real CTOs weigh less than 1 g. However, it is not possible to reduce the mass of the load cell, it is only possible to increase it by attaching different bolts and nuts at its rear thread. By knowing the relationship between efficiency and load cell mass, the graph can be extrapolated to determine the efficiency at the mass of the CTO. In order to simulate this situation, the load cell is hanging freely and it is not connected to the ground, so it is free to move when impacted with its inertia being the only resistance to its acceleration. This would represent the worst case scenario of zero stiffness of the heart tissue. The schematic is shown in figure 5.8.

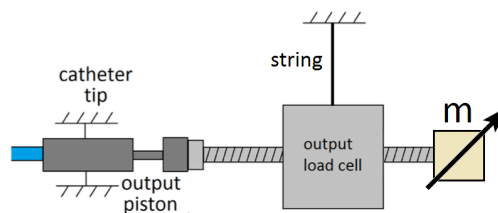


Figure 5.8: Schematic of the setup when the load cell mass is taken into account. The mass of the load cell can be varied by attaching nuts at its rear bolt.

### 5.5.2. Results

The experiments were repeated 3 times each, as there was no need for more since the standard deviation was negligible. For the load cell hanging without any rear attachment (7.2 g), the efficiency was measured to be  $\eta_p = 12.5\%$ . The input peak force remained at the order of 21 N and the pressure wave travelling time at 2.1 N. By attaching different bolts and nuts at the rear attachment, different masses were achieved and used as additional data points. The mass was measured with an electronic balance of 0.01 g precision. The data is plotted on the graph of figure 5.9, setting the intercept at the origin.

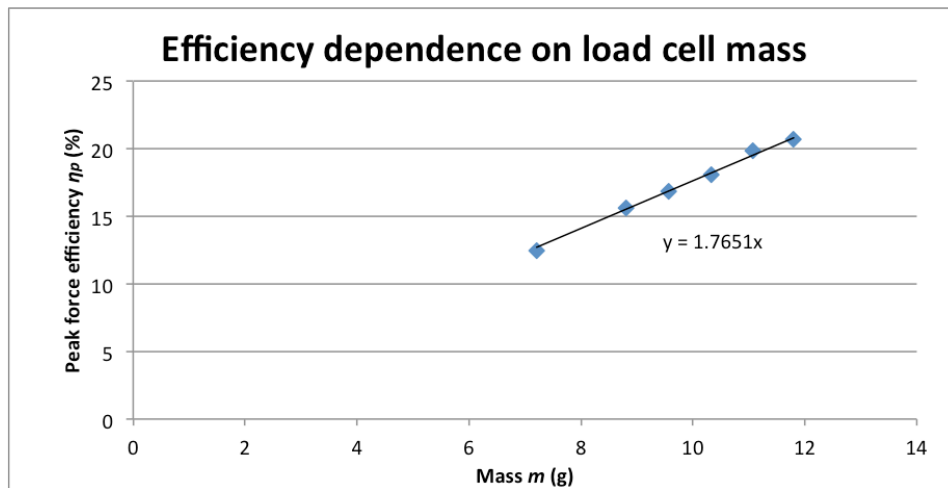


Figure 5.9: Plotted graph of peak force efficiency  $\eta_p$  for different load cell masses  $m$ .

### 5.5.3. Conclusions

The goal of this step is to account for the difference between the load cell mass and the CTO mass. In order to do that, the mass dependence of the efficiency was measured by altering the load cell mass. The conclusion from this experiment is that the higher the mass of the load cell, the more reluctant it is to move when impacted, meaning it gets more of the impacting force due to its resistance to accelerate. This relation is linear and in theory passes through the origin. If we extrapolate the graph of figure 5.9 to the mass of the CTO (say 0.5 g), the efficiency falls to less than 1%, which is very low; for an output force of 2 N, the input should be at least 200 N. Fortunately, the real situation is different because the CTO is attached to the artery walls instead of free hanging, which gives a much higher output force. The question now is how much higher is the efficiency. In order to determine that, all the simulating considerations must be realised at once, as explained in section 5.6.

## 5.6. Artificial CTO replication

After getting a first impression of how simulating the system into a realistic situation alters the results, it was decided to create an artificial CTO replication in order to approximate better its biomechanical properties, meaning its mass, brittleness, hardness and compliance of the heart tissue to which it is attached through the artery walls.

According to Stone et al, CTOs can be soft, hard or contain both hard and soft regions [31]. Usually hard CTOs are characterised by dense fibrous tissue and contain calcified regions. According to Yalonetsky et al, along the CTO length three regions can be identified: the proximal cap, the main body (core) and the distal cap [32]. The proximal cap is a thickened fibrous disc at the proximal end of the occlusion (the first side encountered by the blood flow) and it is the hardest part of the lesion as it contains densely packed collagen and calcified tissue. As a result, this study focuses on penetrating the proximal cap, being the most challenging part of the CTO and the first to be encountered by the catheter tip. Furthermore, unlike acute occlusions, CTOs are strongly connected to the blood vessel wall, which is connected to the cardiac muscle tissue of Young's modulus 100 kPa to 130 kPa [33].

The artificial CTO replication comprises of three parts: the heart tissue / environment, the CTO core and the CTO proximal cap. All three parts should be held in a rectangular container which is tightly fixed on the ground and with a hole on the front side so that the output tip of the device can be inserted. The cylindrical shaped CTO must be surrounded by the environment and in front of the environment a blood mimicking fluid must be present. The proposed concept of the CTO replication in the container being punctured by the device output is shown below (a sharp tip is shown on top of the output piston which is explained later):

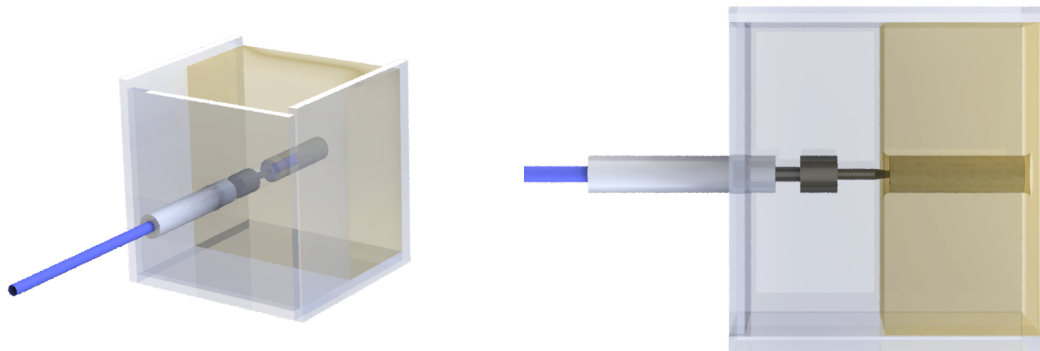


Figure 5.10: Schematic of the proposed concept for puncturing the CTO replication.

In order to mimic the properties of cardiac tissue and CTO material, three components were mixed in the appropriate proportions: gelatin powder (*sheet gelatin*, Dr. Oetker, Bielefeld, Germany), hydroxyapatite referred to as HA ( $CaSO_4$ ; SHERAALPIN Hartgips hellblau, SHERA Werkstoff-Technologie GmbH & Co. KG) and hot water (above  $80^\circ C$ ). A mixture of gelatin powder and hot water is used for the environment. The calcification of the CTO is provided by the HA powder containing calcium sulfate. A mixture of gelatin powder, HA powder and hot water are thus used for the CTO core and cap. The chemical composition of each component is listed in table 5.1:

Component	Gelatin (wt%)	Hydroxyapatite (wt%)	Water (wt%)
Environment (not calcified)	25.00	-	75.00
CTO core (slightly calcified)	16.25	35.00	48.75
CTO cap (heavily calcified)	11.25	55.00	33.75

Table 5.1: Components of the CTO replication and their chemical composition. Qualitatively assessing these components would be a "soft" environment, "slightly harder" CTO core and the CTO caps being the "hardest".

The environment, core and cap had to remain in the refrigerator for 2 hours after mixing so that they attain the required properties. A container made of acrylic plastic and 2 mm thickness was laser cut and glued in order to contain and support the CTO replication. The diameter of the CTO core and cap was chosen to be 5 mm and their length 20 mm and 0.5 mm respectively.

Another aspect that needs to be replicated is the blood environment at the tip. Blood can be mimicked by glycerin diluted in water (25wt% glycerin, 75wt% clear water). The problem is to seal and contain this glycerin solution in front of the CTO cap, surrounding the output tip. To deal with this, a hole was cut in the front plate of the container which would leave a tolerance of 0.2 mm with the output cylinder. Sealing was achieved by the use of vaseline at the tolerance site, since the blood mimicking fluid is not under pressure. The CTO replication is shown in figure 5.11.

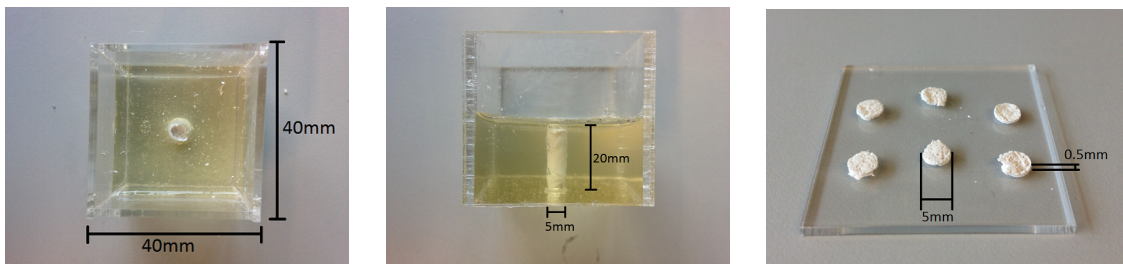


Figure 5.11: Manufactured CTO replication front and side view and CTO caps just taken out of the refrigerator.

For such a cap to be penetrated, a much smaller diameter tip should be impacted upon it. As a result, a 1 mm diameter rod with a filleted tip was glued on top of the impacting piston, as shown in figure 5.12.

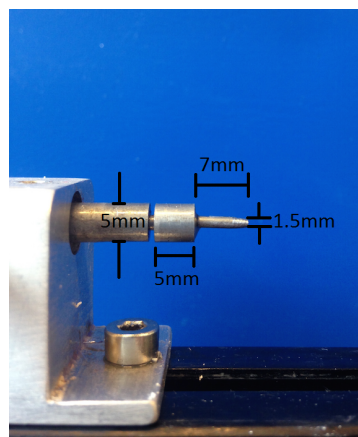


Figure 5.12: New tip attachment for more effective puncturing of the CTO cap.

The aim of this experiment is to puncture the CTO caps effectively, meaning to either break them or penetrate them. Of course, before doing that certain aspects should be considered from the previous findings.

The most important aspect is how much force do we need to puncture the CTO caps. Also, is there a difference in the freshly made caps which are out of the fridge for less than 1 hour (referred to as new caps) against the old ones that have been out of the fridge for more than 24 hours (referred to as old caps). The following experiment was designed: The CTO cap is placed on top of the CTO core inside the container and a load cell with the new tip attachment is pressed against it in a vertical direction. The force measured by the load cell is recorder until fracture occurs.

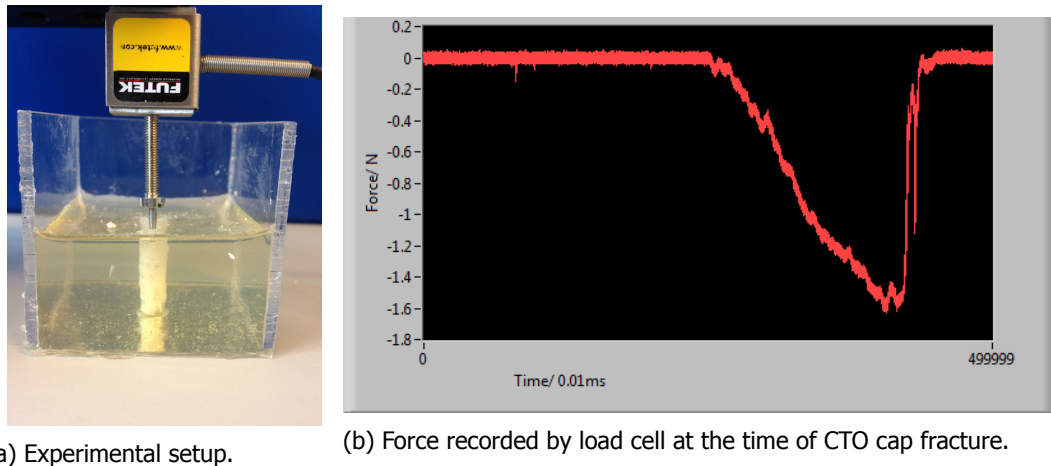


Figure 5.13: Experiment for determining breaking force of CTO caps. The peak indicates cap puncturing. A second sharp tip is observed due to the sudden contact of the CTO with the screw head of the load cell attachment after puncturing.

The results showed an apparent difference between the breaking force of the new and old caps. The new caps required an average force of 1.2 N ( $n = 8$ ,  $SD = 0.4$  N) until fracture while the old ones required 6.2 N ( $n = 8$ ,  $SD = 2.9$  N). This shows that the old caps are more hard and also more brittle, judging by their fracture mode. Most of the new caps were penetrated instead of total fracture. There is also a much wider variation for the breaking force of the old caps, indicated by their larger standard deviation. These results are in accordance with the findings of Thind et al. [34], where forces of the order of 1 N were measured for puncturing occlusions created in rabbit femoral arteries (*ex vivo*).

The four simulating steps taken before are for indicative purposes and although they are not fully consistent with a real scenario they can be used for estimating the required input force to puncture the CTO cap effectively. For this reason, a rough approximation will be used with rounding off the values.

The force efficiency of the initial system without simulation is almost 50%. Introducing a frictionless sliding of the output cylinder through step 1, caused the efficiency to drop to 42%, a factor of **0.84**.

Assuming that the 1.2 N need to be transferred to the back side of the CTO cap, according to step 2 we have an efficiency reduction to 46% for a foam thickness of 0.5 mm. This reduction corresponds to a factor of **0.92**. Of course foam is not the same material as the calcified cap but it can resemble its properties.

In step 3, a spring is introduced. Springs are characterised by a stiffness instead of Young's modulus, so it cannot correspond to the 100 kPa-130 kPa of the heart tissue. However, it is a good indication of introducing compliance to the system. The spring decreased the system efficiency to 24%, a factor of **0.48**. Pre-loading slightly improved the efficiency but it will not be considered for this calculation as its effect is minor and also for a worst-case scenario compensation.

Finally step 4 revealed that the CTO mass affects the efficiency due to its inertia. It also revealed that the efficiency - mass graph is linear and passes through the origin, since for zero mass there would be no output force. The load cell weighs 7.2 g but the CTOs weigh around 2 g. In step 4, the experiment involves a free hanging load cell. In reality the load cell, which resembles the CTO, is attached to the artery walls. For a totally rigid attachment the efficiency is 50%. Assuming linearity and interception through the origin, this would translate to a mass dependence of the efficiency of the form  $\eta_p = (50/7.2)m = 6.9m$ , where the mass  $m$  is in grams. Taking the CTO mass to be 2 g we get an efficiency of 13.8%, a factor of **0.28** of the original system.

All these simulating steps considered together yield a factor of  $0.84 \times 0.92 \times 0.48 \times 0.28 = 0.1$  which shall be multiplied to the reference efficiency of 50% to give 5%. Taking the worst-case scenario, the maximum force needed to break a new CTO cap was measured to be 1.6 N (the average was 1.2 N).

According to this, the input peak force needed is  $1.6/0.05 = 32$  N.

The piston tip was placed in the CTO container and was held by a clamp against it as a replication of the physician's preload. The tube follows a path through the guiding and makes its way in the container, where it is sealed to prevent leaking of the glycerin.

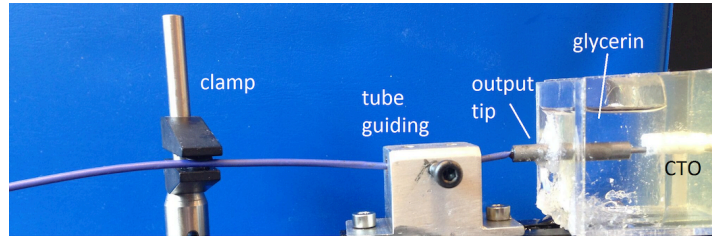


Figure 5.14: Experimental setup at the output side for testing the CTO replication.

The experimental protocol was the following:

- Fill the catheter with water using a syringe while output is at vertical orientation.
- Insert the piston at the output tip and the piston and membrane in the input cylinder, which lies inside the water filled container.
- Turn output tip horizontally and insert it in the CTO replication container.
- Seal the container with vaseline and fill the front side with glycerin solution.
- Clamp softly the tube and push it against the CTO cap.
- Load the impact mechanism and release while the force of the input load cell is measured.
- Take out the CTO cap and check if it is penetrated or broken.

This experiment was done 3 times with the old caps and 5 times with the new. The input peak force was set to around 36 N (with rigid output), 10% more than the estimated force in order to guarantee fracture. The results are summarised in the tables below.

Sample	No. of strikes until puncturing	Input peak force at puncturing strike (N)
1	1	35.7
2	1	36.3
3	1	36.3
4	1	35.4
5	1	35.3

Table 5.2: Number of strikes needed to puncture the new CTO caps. The input force used is around 10% higher than the required force calculated for safety. There is a variation in the input force due to the mechanical actuation of the spring mechanism which produces slightly deviated results.

Sample	No. of strikes until puncturing	Input peak force at puncturing strike (N)
1	2	36.3
2	4	38.5
3	4	37.2

Table 5.3: Number of strikes needed to puncture the old CTO caps.

Since the old caps are more hard, they need more than one strike to be punctured, exhibiting a brittle fracture. The new caps are more soft and are all effectively punctured on the first strike. Their fracture mode is more ductile as they are penetrated and in most of the cases a hole is left in the middle with the rest of the cap remaining almost intact. However, this fracture mode is also desirable since the most common PCI failure mode is the inability to pass a guidewire across the lesion, as stated by Stone et al. [9]. Their softer material is also apparent by the lower input peak force; a more compliant object at the output causes less resistance and a lower impact force at the input.

To conclude, a replication of the real CTO and its surroundings was manufactured out of gelatin and hydroxyapatite and the device was tested on crossing two types of CTO proximal caps, the soft (new) and the hard ones (old). An input force of 36 N was used, as estimated according to previous findings. The softer and more ductile proximal caps are easier to puncture as shown in table 5.2, where all 5 samples are penetrated on the first strike. The reason is that they represent a perfectly inelastic collision, where the two colliding bodies stick together after the impact and the maximum possible kinetic energy is absorbed by the CTO. This was also apparent, as the output tip was skewing through the soft CTO caps, causing them to stick on the edge of the tip. The hard caps required more strikes to be punctured (2 to 4) as indicated by table 5.3 and exhibited a brittle fracture behaviour. Replicating the CTO and conducting this *ex vivo* experiment demonstrated that it is possible to successfully penetrate a real CTO during PCI using the hydraulic pressure wave concept and is encouraging for manufacturing a prototype and proceeding to further research in patients.

# 6

## Target Compliance Sensing

### 6.1. Overview

One aspect of this project is to utilise the existing sensors, in this case the load cells, in order to get useful information in a clinical situation. When the device is used for PCI treatment, one of its major limitations is the inability to know exactly the location of the occlusion. One way to get around this is to inject a dye from the catheter tip in conjunction with exposing the patient to X-rays. However, this solution requires an extra functionality of the catheter and involves the hazards of X-ray usage.

When physicians can avoid the use of X-rays, the standard way of determining the CTO location is simply by inserting the catheter into the patient's arterial system and pushing it forward until it finds its way to the heart. The path length is roughly known, so the physician would expect the catheter to be pushed against the occlusion and resist the forwarding motion. This is normally the indication that the CTO is found, but it might also be that another type of lesion or arterial narrowing or a sudden turn in the tortuous path is on the other side of the device. This could lead to a failed PCI procedure were the occlusion is not treated or even healthy tissue is damaged.

The proposed concept aims to demonstrate that utilising the sensors appropriately can give useful information regarding the nature of the target at the output tip, which could be a calcified CTO, a fatty lesion or an artery wall. The concept can even be extended to the identification of any type of tissue.

### 6.2. Measurement Principle

The principle is based on the idea that the system comprises of many stiffnesses, in parallel and in series to each other. For example, the water inside the tube has its own stiffness, as does the elastic tube wall, the load cell attachment, the membrane etc. It is quite hard to identify each stiffness separately but a change in the total stiffness of the system can be detected under the correct circumstances.

Stiffness can be measured in a static or in a dynamic manner. Statically, a stiffness can be determined by applying a known force and measuring a displacement, or vice versa. Dynamically, stiffness can be measured by exciting the system to its natural frequency and measuring its oscillating frequency or period. For this measurement, a dynamic method is to be used.

The system excitation is provided by the input mechanism which impacts the piston. More specifically, the load cell attachment is used for impacting the piston and also the load cell is used to measure the force between the attachment and the piston. While the attachment provides and impulse to the system, it forces it to resonate. By keeping the load cell attachment in contact with the input piston, one can determine the oscillating period by the rebounding of the piston. This rebounding should not be confused with the reflected pressure wave pulse which travels faster than that; it is caused by the resonating system as a whole.

The appropriate conditions for measuring such a force is to keep contact of the load cell with the resonating system and to have limited damping so that at least the second oscillation is apparent. The limited amount of damping can be achieved by ensuring no air is trapped in the tube. A simplistic way of understanding this principle is to imagine a load cell impacting the end of a fixed spring and measuring its rebounding caused by its resonance.

### 6.3. Experiment

The setup used is the same as before, with the input piston stroke set to 3.5 mm and the upper limit of the mechanism at its loaded position is such that it produces an input peak force of 30 N.

In a situation where the target compliance is to be determined, there would be no sensor at the output tip as the aim is to gain all the useful information just by the input load cell. As a result there is no load cell at the output side of the experiment but there is a spring instead. The spring lies in between the output piston and a rigidly fixed connection. This was facilitated by using appropriate spring mountings, as shown in figure 6.1.



Figure 6.1: Output side of the experiment. A spring is held by a spring mounting between the piston and the rigid wall. The spring is used to simulate the target compliance.

The purpose of the spring is to simulate the compliance of the target tissue. Of course the model is a very simplistic one (single mass-spring system), but it can encourage further research on the topic according to the results. By altering the spring stiffness and keeping all other variables constant, the effect of the force measured by the input load cell can be investigated. A schematic of the whole setup is depicted below:

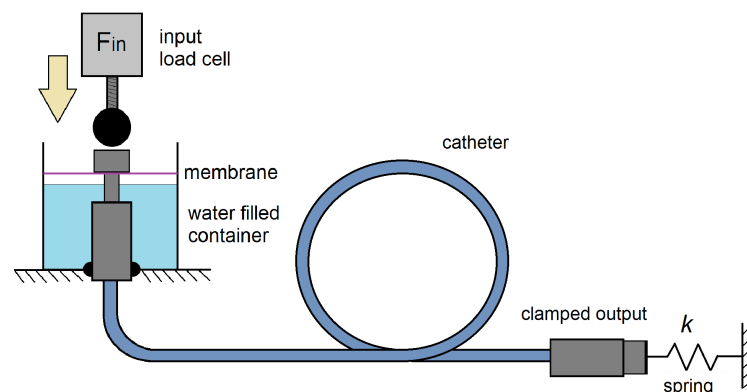


Figure 6.2: Schematic of setup for measuring output target compliance. The input load cell is attached at the tip of the spring actuator (not shown) and hits the input piston with a 30 N peak force

## 6.4. Results

When the experiment was conducted by releasing the impulse mechanism and measuring the load cell force, the typical results were as follows:

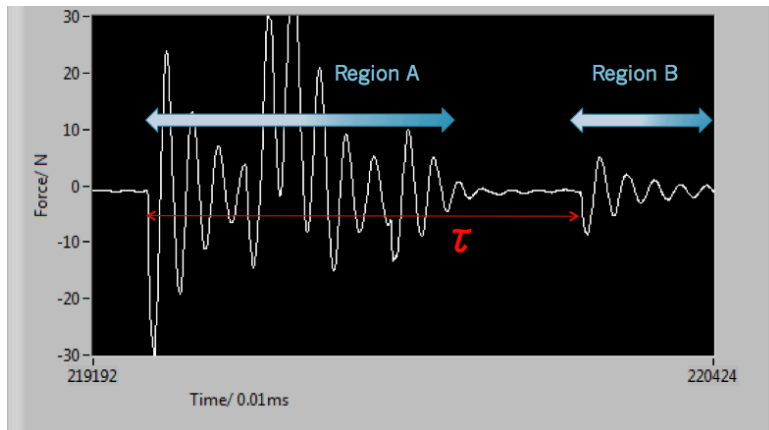


Figure 6.3: Input load cell force measured with the setup of figure 6.2. Two clear regions of sensor ringing (region A and B) where systematically apparent, separated by a time  $\tau$ .

The graph of figure 6.3 clearly shows that the force measured by the load cell exhibits an initial impulse which forces the sensor to resonate (see ringing effect in section 3.3.2). This appears as an asymmetric signal which damps out (region A) and then another signal is measured (region B). The second signal emerges a time  $\tau$  after the initial impulse. This is not the reflected pulse, as it takes a much shorter time for the pressure wave to travel through the tube and back; it was experimentally observed with load cells at both sides that the reflected pulse needs around 4 ms to be detected again at the input. The reflected pulse is most likely inside region A but due to the ringing effect it is not clearly visible. The hypothesis is that the second signal (region B) is caused by the oscillating system, forcing the input piston to rebound back to the load cell and to exert a force on it. In order to verify the hypothesis, two aspects must be investigated:

- The repeatability of the experiment.
- Whether changing the spring stiffness produces a change in the the time  $\tau$ .

Regarding the first point, the experiment was performed 10 times using the ALCOMEX D1680 spring with an indicated stiffness of 2.67 N/mm. The results are shown in table 6.1.

Trial No.	$\tau$ (ms)
1	8.6
2	9.3
3	8.8
4	8.7
5	9.1
6	8.7
7	8.9
8	9.0
9	9.3
10	8.6
<b>AV</b>	<b>8.9</b>
<b>SD</b>	<b>0.3</b>

Table 6.1: Rebounding time  $\tau$  to investigate the repeatability of the experiment for compliance determination.

Since a standard deviation of 0.3 ms is only 3% of the average value of 8.9 s, it can be considered as a quite repeatable experiment. Therefore, the investigation is continued to the second point; whether the spring stiffness has an effect on  $\tau$ .

A spring of the same manufacturer (ALCOMEX DR5370) of indicated stiffness 1.91 N/mm was used as a more compliant case than the previous situation. The experiment was performed again 10 times and the results are summarised in table 6.2.

Trial No.	$\tau$ (ms)
1	9.9
2	10.4
3	10.1
4	10.2
5	9.9
6	9.8
7	10.3
8	10.0
9	10.6
10	10.3
<b>AV</b>	<b>10.2</b>
<b>SD</b>	<b>0.3</b>

Table 6.2: Rebounding time  $\tau$  of a less stiff spring (ALCOMEX DR5370;  $k = 1.91$  N/mm).

The experiment shows again an excellent repeatability and the average value of  $\tau$  has increased to 10.2 ms. Taking into consideration that the period of an oscillating system is inversely proportional to the square root of its stiffness, it makes perfect sense to have a higher period  $\tau$  for a lower spring stiffness. Therefore, the second point is verified as well. The next step is to use a wider variety of stiffnesses and observe the trend of the increasing period  $\tau$  with decreasing stiffness  $k$ .

The springs used were all different models by ALCOMEX: DR5370 (1.91 N/mm), D1680 (2.67 N/mm), DR1960 (3.01 N/mm) and D1910 (7.39 N/mm). The experiments were performed 10 times with each spring. The following graph shows the correlation between the spring stiffness  $k$  and the time period  $\tau$  of the oscillating system. The vertical error bars are included in the graph but are not visible due to their low value.

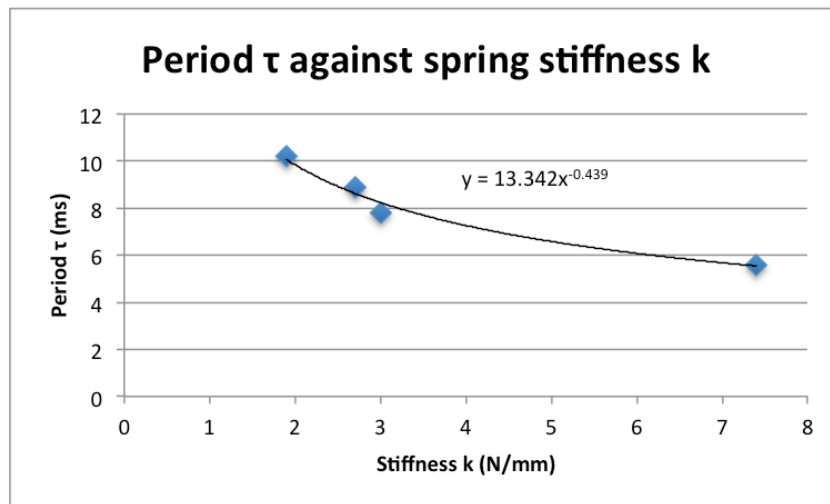


Figure 6.4: Graph showing period  $\tau$  as a function of spring stiffness  $k$ .

A curve has been fitted to the data points as a power function, which exhibits a power of -0.44 with a coefficient of determination equal to  $R^2 = 0.98$ . A fifth data point can be included by performing the experiment without any obstacle at the output. As a result, the piston was free to move forward and the measured force by the input load cell is shown in graph 6.5.

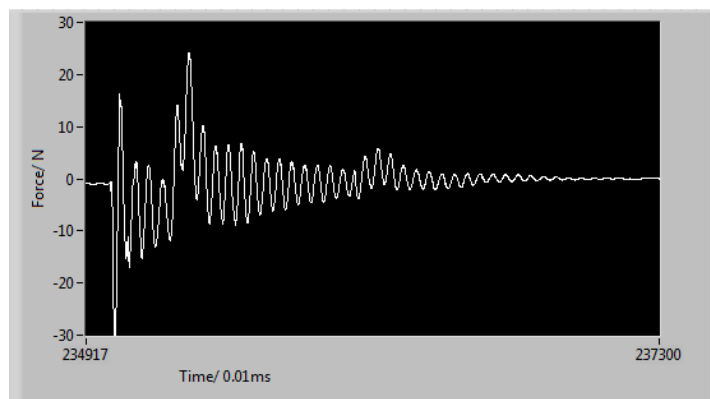


Figure 6.5: Input load cell force without obstacle at the output.

It is clear that there is no rebounding present in this case, as there is no spring connected to a rigid wall to provide a counter-force to the output piston. This situation can be considered as a zero stiffness data point  $k = 0$  where the period  $\tau$  is infinite. Thus, the data point is not defined in graph 6.4. In addition, an experiment was conducted with the output piston hitting a rigid metallic surface, corresponding to a stiffness approaching infinity. The result was a period  $\tau = 4.9$  ms ( $n = 10$ ,  $SD = 0.3$ ). Again this result cannot be plotted on the graph, as the stiffness of the metallic surface is unknown and is probably at a much higher value than the existing data points.

## 6.5. Conclusion and Discussion

In conclusion, the tissue compliance hypothesis has been verified by checking the repeatability of the experiment and by observing a falling trend of period  $\tau$  with spring stiffness  $k$ . This result enables to determine the compliance of the output target just by the signal of the input load cell, which is the goal of this last experiment. However, the stiffness values are based on existing spring parts in the lab and do not represent the target range of compliance, which should be investigated further within a biomedical context.

In the graph of figure 6.4, a power of -0.44 means that the period  $\tau$  is almost proportional to the inverse

of the square root of stiffness  $k$  (proportional would require a power of -0.5). This can be explained theoretically as follows: An undamped resonating system (ideal scenario) is oscillating with a period of  $\tau = 2\pi\sqrt{m/K}$  where  $m$  is its equivalent mass and  $K$  its equivalent stiffness. In this case,  $K$  is the sum of many stiffnesses in series and in parallel, but it can be divided into two basic components: the stiffness of the spring at the output and the stiffness of the rest of the system, connected in series. Assuming that the second stiffness is mostly comprised of the water compressibility, the membrane and the tube elastic modulus, it can be considered much less than the spring stiffness which is of the order of 1 N/mm. As a result,  $K \approx k$  and  $\tau \propto 1/\sqrt{k}$ . In reality, damping and stiffness of the rest of the system alter this result, which is the most likely reason why the power of the fitted curve is -0.44 instead of -0.5.

# 7

## Conclusions and Recommendations

### 7.1. Conclusions

In conclusion, this study achieved to address the limitations of an existing proof-of-concept setup based on the hydraulic pressure wave catheter and replicate a realistic PCI situation for treating CTO. Current state-of-the-art uses mechanical means of energy transfer to puncture cardiac occlusions, which is a major cause of their limited success rate. The hydraulic technology aims to improve the success rate of current devices. The main contribution was to achieve a systematic experimental procedure in order to acquire reliable results. This was done by ensuring a high experimental repeatability, which was the main flaw of the existing setup, through introducing a membrane and a piston stroke adjustment at the input. Furthermore, by immersing the input side in a water container and configuring the output in a horizontal orientation with a limited stroke of less than 4 mm, air entrapment in the system was avoided which was a major improvement, as there is no need to refill the tube at each strike. The main limitations of the existing setup and the way they were tackled are summarised in the following table.

Problem	Solution
Air entrapment in the system	Insert input tip in a water filled container
Impulse is distorted and far from an ideal bell shaped force-time graph	Use appropriate attachment at the impacting load cell
Piston does not retract to original position and input side is exposed	Use a membrane
Weight of output piston causes it to fall and water leaks out	Rotate output to horizontal orientation
Piston stroke is not controlled	Use a height adjustment mechanism to set the input piston stroke

Table 7.1: Summary of problems of the existing setup and how they were tackled using hardware workarounds.

All these modifications enabled to simulate some factors of a realistic situation that were not taken into account previously and study them independently. The factors considered are listed below:

- The sliding of the catheter tip along the artery wall when the device is actuated.
- The piston being in contact with a target surface of same or similar physical properties as a CTO.
- The CTO connection to the heart tissue.

- The mass of the CTO.

Studying these factors gave an indication of how the efficiency of the device is affected in a real situation. The next step was to replicate a CTO and test the device for its feasibility to cross the CTO proximal cap.

The CTO replica model was manufactured using gelatin and hydroxyapatite. Also, two kind of proximal caps were made: soft and hard. The required input force for crossing the caps was estimated and it was demonstrated in a simulated environment that the device can successfully puncture the caps with an average input force of 36 N. More specifically, the hard caps required 2 to 4 strikes whereas for the soft caps a single strike was enough.

The sensing capabilities of the device were also explored. By utilising the input load cell attached to the impact mechanism, it was proved that it is possible to estimate the compliance of the target at the output tip by appropriate calibration. This was a proof-of-concept study and can be used for diagnosis to determine the nature of the tissue which is in contact with the catheter tip without injecting any dye or using medical imaging techniques.

## 7.2. Recommendations

The functionality of the device has been tested on a proof-of-concept setup and the aforementioned conclusions have been drawn but the realisation of a prototype requires more research and optimisation of certain parameters. Based on the research already conducted and the results obtained, the following aspects are recommended to be studied as a continuation of this project in order to build a functional prototype.

### 7.2.1. Effect of pre-load

The effect of pre-load has been evaluated in section 5.4.4, where a pre-load force of 0.6 N produced an average increase in efficiency by 2%. However, the actual pre-load given by the physician is unknown so it is worth investigating how much pre-load is given in a real scenario and how does pre-load alter the efficiency by including more data. Care should be taken, as too much pre-load will defeat the purpose of the hydraulic concept as the tube might be prone to buckling.

### 7.2.2. Effect of trapped air

The problem of air-entrapment was dealt with in the improved setup, both in the input side by immersing the piston into water (section 4.1) and at the output side by rotating the tip to a horizontal orientation (section 4.4). However, it is important to have knowledge of the potential problems. A follow up research path could be to investigate the effect of trapped air in terms of the stiffness and / or damping that it introduces. The biggest challenge would be to quantify the amount of air present in the tube. Possibly a transparent tube might be useful and quantities like the peak force efficiency and pressure wave speed can assess this undesired effect.

### 7.2.3. Pressure measurement

Another aspect that can expand the sensing capabilities of the device is to integrate a pressure sensor. The load cells provide an estimation of the force provided to / by the pistons but they limit this study due to their ringing effect and the forces that arise by contact stresses at impact. As a result, they give a distorted image of the actual situation which can be better approached by introducing pressure measurement. Of course this research direction is a complicated task as an appropriate sensor must be selected in terms of range, resolution and sampling speed. It is also challenging to install such a sensor, as it should be exposed on the water side of the tube (possibly through a T-junction or installed directly at the input cylinder) and its stiffness should be taken into account so that its interference with the measurement is known in advance and accounted for. A question to ask is if the load cell measurements are comparable to the pressure sensor readings and if needed to install multiple sensors along the tube length.

#### 7.2.4. Different actuation method

The current actuation method is a mechanical one using a spring, and this is the reason why there is so much variation in the results of the input peak force. An ideal prototype would need a controlled peak force and piston stroke, both for experimental proof-of-concept purposes and for a certified medical device in the market. This can be achieved by changing the actuation method to an electromagnetic (voice coil) actuator. In this manner, a more accurate peak force can be achieved (less standard deviation) and also one can experiment with different input pulses (pulse shaping). The stroke of the piston can also be adjustable by the actuator by appropriate design. A metallic spherical contact at the actuator impacting tip is preferred over the plastic knob currently used, as it would absorb less energy during impact and would provide a more sharp impulse.

#### 7.2.5. Output modification

Another recommendation is to modify the output tip so that it is suitable for a fully functional prototype. This means that it should be leak proof (currently it is only leak proof due to its orientation) by using a membrane or rubber latex surrounding the tip. Another research direction can study the type, shape and material of the tip and possible manufacturing techniques such as micro-fabrication. The output stroke should be kept to a maximum of 2 mm for safety considerations, so stoppers can be integrated in the mechanical design. Lastly, installing a simple passive spring connecting the piston and cylinder can enable the retracting of the output piston after its impact.

#### 7.2.6. Tissue compliance

Finally, based on the results of chapter 6, follow up research can be conducted by experimenting with real tissue at the output tip and calibrating the device accordingly. This idea can also be used in conjunction with a pressure sensor. Determining the stiffness of the output target gives insight to its nature, which means the device can be used not only for treatment but for diagnosis as well.



# A

## Appendix A: Actuation mechanism

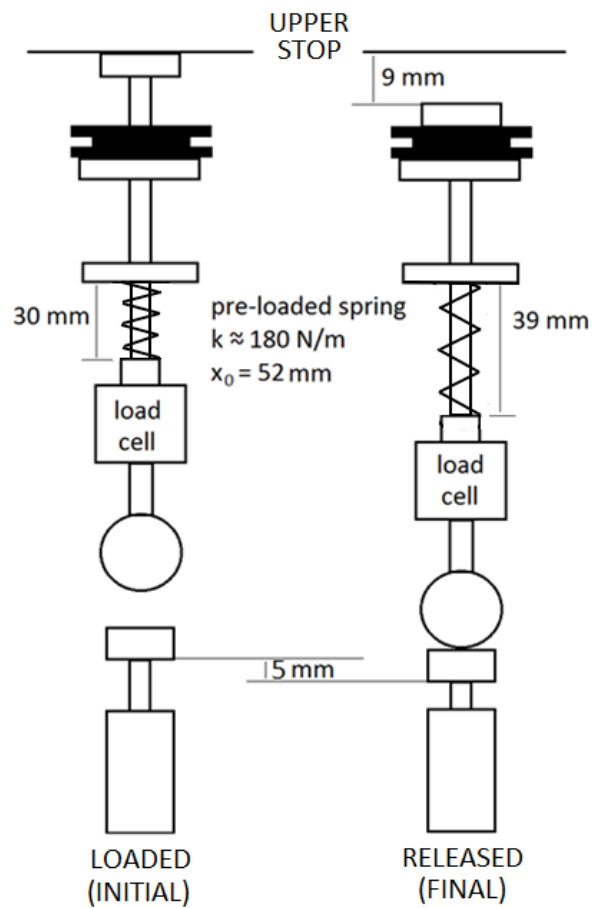


Figure A.1: Schematic of spring mechanism and its relevant dimensions. Piston stroke is set to 5 mm.



# B

## Appendix B: Results with membrane

Trial	$F_{in}$	$F_{out}$	$\eta_p$
1	22.1	11.8	53.4
2	23.5	9.5	40.4
3	18.2	8.8	48.4
4	23.4	10.8	46.2
5	20.1	10.4	51.7
6	25.5	12.8	50.2
7	19.1	9.3	48.7
8	16.3	9.1	55.8
9	17.0	8.5	50.0
10	17.6	9.2	52.3
<b>AV</b>	<b>20.3</b>	<b>10.0</b>	<b>49.7</b>
<b>SD</b>	<b>3.2</b>	<b>1.4</b>	<b>4.3</b>

Table B.1: Experiment for peak force efficiency without membrane.

Trial	$F_{in}$	$F_{out}$	$\eta_p$
1	23.1	11.1	48.1
2	20.9	11.0	52.6
3	22.9	10.9	47.6
4	19.6	10.5	53.6
5	20.6	10.8	52.4
6	22.1	11.2	50.7
7	19.4	10.0	51.5
8	21.4	11.1	51.9
9	22.3	11.6	52.0
10	20.4	9.8	48.0
<b>AV</b>	<b>21.3</b>	<b>10.8</b>	<b>50.8</b>
<b>SD</b>	<b>1.3</b>	<b>0.6</b>	<b>2.2</b>

Table B.2: Experiment for peak force efficiency with membrane.

# C

## Appendix C: CTO and device modelling results

No Modelling				
Trial	$F_{in}$ (N)	$F_{out}$ (N)	$\eta_p$ (%)	$\Delta t$ (ms)
1	20.5	9.2	44.9	2.0
2	21.5	11.2	52.1	2.0
3	18.1	9.2	50.8	2.0
4	21.7	11.6	53.5	1.9
5	20.8	10.8	51.9	1.8
6	18.2	9.4	51.6	1.9
7	21.9	10.7	48.9	1.9
8	21.2	10.4	49.1	1.8
9	19.4	9.8	50.5	2.1
10	21.8	10.9	50.0	1.9
11	20.2	10.7	53.0	2.0
12	21.5	10.5	48.8	1.8
13	19.8	9.8	49.5	1.9
14	19.3	9.6	49.7	1.9
15	20.8	10.6	51.0	2.0
16	19.8	9.7	49.0	2.0
17	21.6	10.8	50.0	1.8
<b>AV</b>	<b>20.5</b>	<b>10.3</b>	<b>50.3</b>	<b>1.9</b>
<b>SD</b>	<b>1.2</b>	<b>0.7</b>	<b>2.0</b>	<b>0.1</b>

Table C.1: Results without any modelling.

Step 1: sliding cylinder				
Trial	$F_{in}$ (N)	$F_{out}$ (N)	$\eta_p$ (%)	$\Delta t$ (ms)
1	20.2	8.6	42.6	1.9
2	20.8	9.1	43.8	2.1
3	19.6	9.3	47.4	2.0
4	21.2	9.7	45.8	1.9
5	21.2	10.1	47.6	1.9
6	18.9	7.9	41.8	2.0
7	19.1	7.9	41.4	2.0
8	22.1	9.9	44.8	2.0
9	20.8	8.6	41.3	2.0
10	21.1	9.5	45.0	1.9
11	20.1	8.4	41.8	2.1
12	22.3	9.7	43.5	2.1
13	21.4	7.6	35.5	2.0
14	19.1	6.8	35.6	2.0
15	19.4	8.7	44.8	2.0
16	22.2	10.3	46.4	1.9
17	20.8	7.9	38.0	2.0
<b>AV</b>	<b>20.6</b>	<b>8.8</b>	<b>42.8</b>	<b>2.0</b>
<b>SD</b>	<b>1.1</b>	<b>1.0</b>	<b>3.7</b>	<b>0.1</b>

Table C.2: Results for first modelling step.

Step 2: Foam of $t = 2$ mm thickness in between the piston and the load cell				
Trial	$F_{in}$ (N)	$F_{out}$ (N)	$\eta_p$ (%)	$\Delta t$ (ms)
1	20.2	7.1	35.1	2.2
2	20.1	7.8	38.8	2.3
3	19.3	5.7	29.5	2.3
4	18.2	6.2	34.1	2.4
5	19.1	6.3	33.0	2.3
6	21.7	7.0	32.3	2.4
7	22.3	7.1	31.8	2.2
8	20.0	7.5	37.5	2.2
9	19.4	6.9	35.6	2.4
10	19.7	6.8	34.5	2.2
11	20.4	6.5	31.9	2.3
12	18.3	7.3	39.9	2.3
13	20.9	6.4	30.6	2.2
14	19.3	5.9	30.6	2.5
15	22.0	8.1	36.8	2.2
16	19.1	6.1	31.9	2.1
17	18.4	6.4	34.8	2.3
<b>AV</b>	<b>19.9</b>	<b>6.8</b>	<b>34.0</b>	<b>2.3</b>
<b>SD</b>	<b>1.2</b>	<b>0.7</b>	<b>3.0</b>	<b>0.1</b>

Table C.3: Results for second modelling step with  $t = 2$  mm.

Step 2: Foam of $t = 3$ mm thickness in between the piston and the load cell				
Trial	$F_{in}$ (N)	$F_{out}$ (N)	$\eta_p$ (%)	$\Delta t$ (ms)
1	21.9	6.7	30.6	2.2
2	20.4	5.1	25.0	2.3
3	19.7	5.2	26.4	2.2
4	21.3	5.9	27.7	2.5
5	20.2	6.1	30.2	2.3
6	19.8	5.1	25.8	2.4
7	19.4	5.8	29.9	2.5
8	20.1	5.4	26.7	2.3
9	19.1	6.0	31.4	2.2
10	18.5	4.7	25.4	2.4
11	19.9	5.4	27.1	2.2
12	18.8	5.8	30.9	2.5
13	19.4	5.6	28.9	2.4
14	21.2	6.3	29.7	2.4
15	18.3	4.2	23.0	2.2
16	21.7	6.8	31.3	2.3
17	20.9	5.9	28.2	2.3
<b>AV</b>	<b>20.0</b>	<b>5.6</b>	<b>28.1</b>	<b>2.3</b>
<b>SD</b>	<b>1.1</b>	<b>0.7</b>	<b>2.5</b>	<b>0.1</b>

Table C.4: Results for second modelling step with  $t = 3$  mm.

Step 2: Foam of $t = 4$ mm thickness in between the piston and the load cell				
Trial	$F_{in}$ (N)	$F_{out}$ (N)	$\eta_p$ (%)	$\Delta t$ (ms)
1	18.4	5.1	27.7	2.3
2	19.8	4.7	23.7	2.3
3	19.4	5.3	27.3	2.5
4	18.5	3.9	21.1	2.6
5	21.4	5.8	27.1	2.2
6	20.8	4.1	19.7	2.2
7	20.9	4.0	19.1	2.3
8	18.8	4.1	21.8	2.4
9	19.5	5.2	26.7	2.3
10	20.8	4.8	23.1	2.3
11	22.1	6.1	27.6	2.4
12	19.8	3.9	19.7	2.3
13	19.1	5.1	26.7	2.3
14	18.2	4.2	23.1	2.1
15	21.6	5.8	26.9	2.2
16	18.7	4.7	25.1	2.4
17	19.4	4.4	22.7	2.3
<b>AV</b>	<b>19.8</b>	<b>4.8</b>	<b>24.1</b>	<b>2.3</b>
<b>SD</b>	<b>1.2</b>	<b>0.7</b>	<b>3.0</b>	<b>0.1</b>

Table C.5: Results for second modelling step with  $t = 4$  mm.

Step 2: Foam of $t = 6$ mm thickness in between the piston and the load cell				
Trial	$F_{in}$ (N)	$F_{out}$ (N)	$\eta_p$ (%)	$\Delta t$ (ms)
1	21.2	4.5	21.2	2.5
2	18.9	5.1	27.0	2.4
3	20.5	4.2	20.5	2.4
4	20.9	4.3	20.6	2.2
5	18.3	3.9	21.3	2.3
6	22.5	5.1	22.7	2.3
7	20.1	4.9	24.4	2.1
8	19.7	3.8	19.3	2.3
9	19.5	4.2	21.5	2.4
10	19.4	4.9	25.3	2.1
11	20.8	4.0	19.2	2.4
12	21.2	4.8	22.6	2.3
13	19.4	3.9	20.1	2.3
14	20.2	3.6	17.8	2.2
15	22.1	5.6	25.3	2.3
16	21.9	4.4	20.1	2.1
17	18.8	4.5	23.9	2.3
<b>AV</b>	<b>20.3</b>	<b>4.5</b>	<b>21.9</b>	<b>2.3</b>
<b>SD</b>	<b>1.2</b>	<b>0.5</b>	<b>2.5</b>	<b>0.1</b>

Table C.6: Results for second modelling step with  $t = 6$  mm.

Step 3: Spring between load cell and wall (no preload)				
Trial	$F_{in}$ (N)	$F_{out}$ (N)	$\eta_p$ (%)	$\Delta t$ (ms)
1	17.8	4.4	24.7	1.9
2	18.8	5.0	26.6	2.1
3	16.6	4.3	25.9	2.1
4	16.2	5.0	30.9	2.0
5	19.5	4.5	23.1	1.8
6	18.7	4.8	25.7	1.9
7	18.3	5.3	29.0	2.2
8	21.1	4.4	20.9	2.0
9	19.9	4.6	23.1	2.0
10	20.6	4.6	22.3	2.1
11	22.3	4.1	18.4	2.0
12	18.5	3.9	21.1	1.8
13	19.6	6.6	33.7	1.9
14	19.8	4.3	21.7	1.9
15	19.4	4.7	24.2	2.1
16	20.6	3.2	15.5	2.0
17	17.5	4.4	25.1	2.1
<b>AV</b>	<b>19.1</b>	<b>4.6</b>	<b>24.2</b>	<b>2.0</b>
<b>SD</b>	<b>1.6</b>	<b>0.7</b>	<b>4.4</b>	<b>0.1</b>

Table C.7: Results for third modelling step without preload.

Step 3: Spring between load cell and wall (0.6 N preload)				
Trial	$F_{in}$ (N)	$F_{out}$ (N)	$\eta_p$ (%)	$\Delta t$ (ms)
1	19.8	5.2	26.3	2.1
2	22.3	6.5	29.1	2.1
3	20.4	5.7	27.9	2.0
4	20.9	5.5	26.3	2.1
5	22.0	6.2	28.2	1.9
6	18.9	5.0	26.5	1.8
7	20.1	5.7	28.4	1.9
8	19.7	4.7	23.9	2.0
9	19.5	4.8	24.6	2.1
10	21.4	4.9	22.9	2.0
11	20.9	5.3	25.4	1.8
12	22.4	5.9	26.3	1.9
13	18.5	5.6	30.3	2.1
14	21.9	4.9	22.4	1.9
15	21.8	5.2	23.9	1.9
16	19.6	5.7	29.1	2.0
17	22.3	6.1	27.4	2.1
<b>AV</b>	<b>20.7</b>	<b>5.5</b>	<b>26.4</b>	<b>2.0</b>
<b>SD</b>	<b>1.3</b>	<b>0.5</b>	<b>2.3</b>	<b>0.1</b>

Table C.8: Results for third modelling step with 0.6 N preload.

# D

## Appendix D: Tissue compliance results

DR5370 (1.91 N/mm)	
Trial	$\tau$ (ms)
1	9.9
2	10.4
3	10.1
4	10.2
5	9.9
6	9.8
7	10.3
8	10.0
9	10.6
10	10.3
<b>AV</b>	<b>10.2</b>
<b>SD</b>	<b>0.3</b>

Table D.1: Time  $\tau$  for ALCOMEX DR5370 (1.91 N/mm).

D1680 (2.67 N/mm)	
Trial	$\tau$ (ms)
1	8.6
2	9.3
3	8.8
4	8.7
5	9.1
6	8.7
7	8.9
8	9.0
9	9.3
10	8.6
<b>AV</b>	<b>8.9</b>
<b>SD</b>	<b>0.3</b>

Table D.2: Time  $\tau$  for ALCOMEX D1680 (2.67 N/mm).

DR1960 (3.01 N/mm)	
Trial	$\tau$ (ms)
1	8.0
2	8.2
3	8.0
4	7.3
5	7.5
6	7.7
7	7.4
8	8.1
9	7.9
10	8.1
<b>AV</b>	<b>7.8</b>
<b>SD</b>	<b>0.3</b>

Table D.3: Time  $\tau$  for ALCOMEX DR1960 (3.01 N/mm).

D1910 (7.39 N/mm)	
Trial	$\tau$ (ms)
1	5.2
2	5.8
3	5.9
4	4.9
5	5.9
6	5.5
7	5.4
8	5.7
9	6.0
10	5.4
<b>AV</b>	<b>5.6</b>
<b>SD</b>	<b>0.4</b>

Table D.4: Time  $\tau$  for ALCOMEX D1910 (7.39 N/mm).



# Bibliography

- [1] World Health Organisation, *Cardiovascular Diseases (CVDs)*, <http://www.who.int/mediacentre/factsheets/fs317/en/>, accessed: 06-9-2017.
- [2] National Heart, Lung and Blood Institute, *What Are the Signs and Symptoms of Coronary Heart Disease?* <https://www.nhlbi.nih.gov/health/health-topics/topics/cad/signs> (), accessed: 18-9-2017.
- [3] J. Jameson, D. Kasper, T. Harrison, E. B. A. Fauci, S. Hauser, and D. Longo, *Harrison's principles of internal medicine* (McGraw-Hill Medical Publishing Division, New York, 2005).
- [4] *Coronary Artery Disease Essay*, <https://sites.google.com/site/cardiovascularbiotech/coronary-artery-disease-essay>, accessed: 19-9-2017.
- [5] F. Zidar, B. Kaplan, W. O'Neill, D. Jones, T. Schreiber, R. Safian, S. Ajluni, J. Sobolski, G. Timmis, and C. Grines, *Prospective, randomized trial of prolonged intracoronary urokinase infusion for chronic total occlusions in native coronary arteries*, *Journal of the American College of Cardiology* **27**, 1406 (1996).
- [6] J. Ge, *Current status of percutaneous coronary intervention of chronic total occlusion*, *Journal of Zhejiang University SCIENCE B* **13**, 589 (2012).
- [7] National Heart, Lung and Blood Institute, *Percutaneous Coronary Intervention*, <https://www.nhlbi.nih.gov/health/health-topics/topics/angioplasty> (), accessed: 19-9-2017.
- [8] D. Darling, *Cardiac catheterization*, [http://www.daviddarling.info/encyclopedia/C/cardiac\\_catheterization.html](http://www.daviddarling.info/encyclopedia/C/cardiac_catheterization.html), accessed: 22-9-2017.
- [9] G. Stone, N. Reifart, I. Moussa, A. Hoye, D. Cox, A. Colombo, D. Baim, P. Teirstein, B. Strauss, M. Selmon, G. Mintz, O. Katoh, K. Mitsudo, T. Suzuki, H. Tamai, E. Grube, L. Cannon, D. Kandzari, M. Reisman, R. Schwartz, S. Bailey, G. Dangas, R. Mehran, A. Abizaid, J. Moses, M. Leon, and P. Serruys, *Percutaneous recanalization of chronically occluded coronary arteries: a consensus document: part ii*, *Circulation* **112**, 2530 (2005).
- [10] A. Sakes, T. Nicolai, J. Karapanagiotis, P. Breedveld, and J. Spronck, *Crossing total occlusions using a hydraulic pressure wave: A feasibility study*, (2017), unpublished, submitted to Nature Biomedical Engineering.
- [11] T. Nicolai, *Puncturing chronic total occlusions using hydraulic pressure waves*, Master's thesis, Delft University of Technology (2017).
- [12] E. Brilakis, J. Grantham, S. Rinfert, M. Wyman, M. Burke, D. Karpaliotis, N. Lembo, A. Pershad, D. Kandzari, C. Buller, T. DeMartini, W. Lombardi, and C. Thompson, *A percutaneous treatment algorithm for crossing coronary chronic total occlusions*, *JACC: Cardiovascular Interventions* **5**, 367 (2012).
- [13] R. Osnabrugge, E. Magnuson, P. Serruys, C. Campos, K. Wang, D. van Klaveren, V. Farooq, M. Abdallah, H. Li, K. Vilain, E. Steyerberg, M. Morice, K. Dawkins, F. Mohr, A. Kappetein, and D. Cohen, *Cost-effectiveness of percutaneous coronary intervention versus bypass surgery from a dutch perspective*, *Heart* **101**, 1980 (2015).
- [14] P. U. Prashant, *Current and emerging catheter technologies for percutaneous transluminal coronary angioplasty*, *Research Reports in Clinical Cardiology* **2014**, 213 (2014).

- [15] Encyclopedia Britannica, *Balloon angioplasty*, <https://www.britannica.com/topic/balloon-angioplasty>, accessed: 22-9-2017.
- [16] Merriam-Webster, *Definition of recanalization*, <https://www.merriam-webster.com/dictionary/recanalization>, accessed: 08-10-2017.
- [17] BARD Peripheral Vascular, *Crosser CTO Recanalization Catheters*, <http://www.bardpv.com/portfolio/crossercto/>, accessed: 09-10-2017.
- [18] Cordis - A Cardinal Health Company, *Frontrunner XP CTO Catheter*, <https://emea.cordis.com/emea/endovascular/lower-extremity-solutions/cross/frontrunner-xp-cto-catheter.html>, accessed: 09-10-2017.
- [19] Avinger, *KittyCat2*, <http://avinger.com/devices/kittycat/>, accessed: 09-10-2017.
- [20] J. Gukler, L. Bansemir, H. Klues, and A. Bufe, *Chronic total coronary occlusion recanalization: Current techniques and new devices*, *Journal of the Saudi Heart Association* **29**, 110 (2017).
- [21] A. Sakes, M. van der Wiel, D. Dodou, and P. Breedveld, *Endovascular crossing of chronic total occlusions using an impulse: An explorative design study*, *Cardiovascular Engineering and Technology* **8**, 145 (2017).
- [22] M. H. Chaudhry, *Applied Hydraulic Transients (3rd ed.)* (Springer, New York, 1987).
- [23] A. Tijsseling and A. Anderson, *A. Isebre Moens and D.J. Kortweg on the speed and propagation of waves in elastic tubes*, Master's thesis, Eindhoven University of Technology and School of Mechanical and Systems Engineering University of Newcastle upon Tyne.
- [24] A. Chatterjee, *Rigid body collisions: some general considerations, new collision laws, and some experimental data*, Master's thesis (1997).
- [25] J. Peraire and S. Widnall, *Lecture L9 - Linear Impulse and Momentum. Collisions*, (2009).
- [26] L. Forney, *On the duration of contact for the hertzian impact of a spherical indenter on a maxwell solid*, *International Journal of Solids and Structures* **10**, 621 (1974).
- [27] D. Hanaor, Y. Gan, and I. Einav, *Contact mechanics of fractal surfaces by spline assisted discretisation*, *International Journal of Solids and Structures* **59**, 121 (2015).
- [28] Sparkfun Electronics, *Getting started with load cells*, <https://learn.sparkfun.com/tutorials/getting-started-with-load-cells>, accessed: 12-9-2017.
- [29] Precision Weighing Balances, *Strain Gauge Transducer*, <http://www.scalenet.com/applications/glossary.html>, accessed: 12-9-2017.
- [30] Giri Brothers, *S-Type*, <https://giribrothers.in/component/virtuemart/browse/146-s-type.html?sef=hc&vmcchk=1>, accessed: 12-9-2017.
- [31] G. Stone, N. Reifart, I. Moussa, A. Hoye, D. Cox, A. Colombo, D. Baim, P. Teirstein, B. Strauss, M. Selmon, G. Mintz, O. Katoh, K. Mitsudo, T. Suzuki, H. Tamai, E. Grube, L. Cannon, D. Kandzari, M. Reisman, R. Schwartz, S. Bailey, G. Dangas, R. Mehran, A. Abizaid, J. Moses, M. Leon, and P. Serruys, *Percutaneous recanalization of chronically occluded coronary arteries: a consensus document: part i*, *Circulation* **112**, 2364 (2005).
- [32] S. Yalonetsky, A. Osherov, B. Strauss, R. Galassi, S. Tomasello, and H. Khamis, *Chronic Total Occlusions. A guide to Recanalization (2nd ed.)* (Willey-Blackwell, Hoboken, 2013).
- [33] R. Houwink and H. D. Decker, *Elasticity, plasticity and structure of matter* (Cambridge University Press, Cambridge, 1971).
- [34] A. Thind, B. Strauss, A. Teitelbaum, R. Karshafian, M. Ladouceur, C. Whyne, D. Goertz, and S. Foster, *A novel method for the measurement of proximal fibrous cap puncture force in chronic total occlusions: the effect of increasing age*, *EuroIntervention (Official Journal of EuroPCR and European Association of Percutaneous Cardiovascular Interventions)* **6** (2011), 10.4244/EIJV6I8A172.

- [35] H. Kahraman, M. Ozaydin, E. Varol, S. Aslan, A. Dogan, A. Altinbas, M. Demir, O. Gedikli, G. Acar, and O. Ergene, *The diameters of the aorta and its major branches in patients with isolated coronary artery ectasia*, *Texas Heart Institute Journal* **33**, 463 (2006).
- [36] B. Scientific, *Impulse diagnostic catheter*, <http://www.bostonscientific.com/en-US/products/catheters--diagnostic/impulse-diagnostic-catheter.html>, accessed: 14-9-2017.
- [37] F. Faul, E. Erdfelder, A. Buchner, and A. Lang, *Statistical power analyses using G\*power 3.1: Tests for correlation and regression analyses*, *Behavior Research Methods* **41**, 1149 (2009).